Fall 2018

Topological Conduction and Investigation on Multi Occurrence of Dirac Cone

Mustahseen Mobashwer Indaleeb

TOPOLOGICAL CONDUCTION AND INVESTIGATION ON MULTI OCCURRENCE OF DIRAC CONE

by

Mustahseen Mobashwer Indaleeb

Bachelor of Science
Military Institute of Science & Technology, 2013

Submitted in Partial Fulfillment of the Requirements

For the Degree of Master of Science in

Mechanical Engineering

College of Engineering and Computing

University of South Carolina

2018

Accepted by:

Sourav Banerjee, Director of Thesis

Tanvir Farouk, Reader

Cheryl L. Addy, Vice Provost and Dean of the Graduate School

DEDICATION

This work is dedicated to my friends and family.

ACKNOWLEDGEMENTS

I would like to express my deep gratitude and thanks to my advisor Dr. Sourav Banerjee, Associate Professor, University of South Carolina for his guidance, invaluable suggestions, constructive criticisms and sharing his knowledge throughout this work. It has been a great privilege and honor for me to work with him. I would also like to thank Dr. Tanvir I Farouk, Associate Professor, University of South Carolina, for his precious concern in this research and kindly agreeing to officially serve as the reader. I would like to express my gratitude to Dr. Md Riaz U Ahmed, Assistant Professor, University of Wisconsin - Green Bay, for guiding me towards this research and helping me in every aspect. I would also like to thank all the members of iMAPS (Integrated Material Assessment and Predictive Simulation) for their guidance in my progress, especially Hossain Ahmed and Sadegh Saadatzi for their kind support. Finally, special thanks go to my wife, my parents and my in-laws for their support and encouragements to achieve this goal.

ABSTRACT

The unique phenomena in acoustic metamaterial at the Dirac-like cone, and at the exceptional spawning ring could transform the field of engineering with multiple new applications that were never possible before. Localized conical dispersion called Dirac cone at the Brillouin Zone boundaries are the well-known phenomena demonstrated by photonics and phononic metamaterials. However, Dirac cone-like dispersion at the center of the Brillouin zone (where wave number, k = 0) [1] is rare and only happens due to accidental degeneracy at finite frequencies in two-dimensional periodic crystals (PCs), with or without microarchitectures. Accidental degeneracies are generally the 'sweet spots' where the time-reversal symmetry of the material breaks down and might have tremendous applications in engineering, which are not fully realized yet. Additionally, unlike Topological insulators, which is one of the most currently discussed topics in condensed matter physics, we have developed an acoustic topological conductor which helps to conduct acoustic pressure energy along the crystals, keeping the topology protected. Exploiting these behaviors of Dirac cones and spawning rings at the origin and boundaries of the Brillouin zone, a directional and bifurcation lens were designed which will propagate sound wave in specific directions at multiple frequencies.

In this study, it is shown that even simplest geometrical microarchitecture of the Phononic Crystals (PnCs) in a periodic structure can be modulated to obtain the accidental degeneracies at different frequencies, while the frequency of a nondispersive 'deaf' band'

obtained from any arbitrary periodic structure made of similar PnCs remains unaltered. Exploiting this behavior of the Dirac cones at the origin of the Brillouin zone, a 'deaf band' based predictive modulations of the PnCs are realized and multiple occurrences of the Dirac like points are demonstrated.

Moreover, a formation of dual Dirac cones at the center of the Brillouin zone, at different frequencies has also never been reported in the literature. Generation of multiple Dirac like cones at the center and the edge of a Brillouin zone, which is rare and, usually, non-manipulative is also demonstrated in this article. By deploying variable angular position of the square PVC resonator as a unit cell in a phononic crystals (PC) system, the locations of the degenerated double Dirac cones have been manipulated at various frequency points. A baseline periodic structure having a square array of cylindrical polyvinylchloride (PVC) inclusions in air media is studied numerically in this study, which was previously studied for band gaps and wave bifurcation. Detailed numerical study of the PnCs showed that by predictively adjusting the PnCs parameters, even an accidental triple degeneracy of dispersion at Γ point ($k = 0$) can be achieved. The claims were further validated using numerical experiments on a metamaterial slab composed of designed PnCs which demonstrates the unique Dirac cone phenomena e.g. orthogonal wave transport, negative refractive index material, and wave vortex.

TABLE OF CONTENTS

LIST OF FIGURES

LIST OF SYMBOLS

$\sigma_{nl,l}$	derivative of stress with respect to l^{th} direction
f_n	Body force in n^{th} direction
ρ	density of the material
$\ddot{u_n}$	acceleration in n^{th} direction
δ	Kronecker Delta
$\vec{G_i}$	Reciprocal lattice vectors
D_i or a	Lattice constant of unit cell
ζ_i	Volume fraction of the respective constituent media
J_1	Bessel function of the 1^{st} kind
r	Radius of the PVC rod
ω or f	Frequency
$\vec{k}$	Wave vector
M	Corner point along the top-right edge of the Brillouin zone.
Γ	Center point of Brillouin zone.
X	Last point at the right boundary along horizontal straight line from center of BZ
C_i	Channel number for numerical analysis model
S	Side length of square resonator
θ	Angle of rotation

LIST OF ABBREVIATIONS

BF…….. Bloch-Floquet

BZ…….. Brillouin Zone

IT…….……... Incident Transmission

OT……...…….. Orthogonal Transmission

PnC……. Phononic crystal

PVC…… Polyvinyl-Chloride

PWE…….. Plane Wave Expansion

CHAPTER 1

INTRODUCTION

Wave dispersion behavior at Dirac frequencies enables capabilities of extraordinary wave transport and manipulation of the acoustical waves [1-5]. Dirac frequencies are identified from the dispersion curves in specially designed periodic media called metamaterials. Dirac points can occur at the Brillouin boundary [1] or at the center of the Brillouin zone [6], identified in a reciprocal wave number space (k) in a periodic media. In photonics that concerns electromagnetic waves, exhibits Dirac phenomenon at the Fermi level, were energy, E is linearly proportional to the electromagnetic wave vector k. As the Dirac equation describes relativistic spin ½ particles, the band structure near fermi level at the hexagonal corners of Graphene exhibits linear Dirac dispersion and is explained by massless Dirac equation [7]. This point is called the Dirac point and the conical shaped [7] dispersion pattern is called the Dirac cone. Dirac cone at Brillouin boundary exhibits electronic transport phenomena like, Zitterbewegung oscillation [8], Klein tunneling [9, 10], anti-localization [11, 12] and integer quantum Hall effect [13]. These behaviors resulted the breaking of the time reversal symmetry and also helped to find zero refractive index materials [14]. Researchers have realized and experimentally proved these behaviors in photonic crystals in presence of external magnetic field. However, limited activities can be found in phononics, where alternative to a magnetic field does not exists.

Despite this fact, Dirac cones were found at the intersection of two bands at the corners of the Brillouin Zone, when triangular and hexagonal honeycomb periodic phononics metamaterial were designed. Dirac cones in PnCs were first shown in 2008 [1], which was at the X/M point (at the boundary of the Brillouin zone) having a double degeneracy. Few other researchers reported that the Dirac cones also yield phenomena like object cloaking [6], and super-anisotropy [2, 3]. Researchers used two-dimensional PnCs and through transmission of acoustic waves near Dirac point they found the pseudo-diffusion behavior and Zitterbewegung effect, equivalent to photonics present in acoustics. As the phenomena from photonics are replicated in phononics, it is realized that the phononics should also have accidental degeneracies at the center of the Brillouin Zone (i.e. $@\ \vec{k} = 0$), like it was reported in photonics[15, 16]. Recently finding a Dirac cone at the center of the Brillouin Zone has become a challenge. It has been found that at the center of the Brillouin Zone accidental degeneracy may result a triple degenerate eigenstate, having two linear bands forming a cone, and a flat band, which is a conical singularity, intersecting them at the center of the Brillouin Zone [6]. Despite having linear bands for both Dirac points at the Brillouin boundary and at the center of the Brillouin zone, they apparently do not reflect the same physics. Dirac point at the center of the Brillouin Zone occurs due to accidental degeneracy but Dirac cone at Brillouin Zone boundary occurs due to deterministic degeneracy. That is why the point at Brillouin Zone boundary is called Dirac point and the linear dispersion is called Dirac cone. Whereas the point at the center of the Brillouin Zone is called the “Dirac-like point” and the dispersion cone is called the ‘Dirac-like cone” [2, 4].

In photonics, researchers proposed the first-principles theory by studying the Dirac–like cone dispersion at any symmetric point in the Brillouin zone, independent of frequency and lattice structure [4]. A theoretical model was developed to predict the existence of the linear dispersion. For photonic crystal, a non-zero, mode coupling integral between the degenerate Bloch states guarantees Dirac-like point, regardless of the type of degeneracy[17]. Recently, a study has been conducted with phononics on tunable topological PnCs where Dirac–like cone was generated by tuning the physical parameter. To simulate the quantum Hall effect (topological insulator) equivalent to the spinning electrons inside the material and propagating the waves around the boundary of the material block, they proposed circular air duct PnCs where air flow can be rotated by injecting forced air flow inside due to the absence of the magnetic field in phononics[18, 19]. It was a successful attempt but complicated. However, it is argued that if with a simplest baseline PnCs (which are already established for band gap study), is it possible to design the geometry of the PnCs without injecting forced air flow but still can predictively generate a Dirac-like cone. It is found that pivoting on the 'deaf-band' this prediction is possible even in a simplest PnCs system, presented in this article.

In this article we considered a simple arrangement of cylindrical Polyvinyl Chloride (PVC) rods as PnCs immersed in air that was previously studied for band gaps and wave bifurcation[20-22]. With a C_{4v} symmetry, the lattice constant of the unit cell was considered as, $a = 1$ *inch*. The initial arbitrary radius of the resonator was set to $r = 0.193a$. Density, Young's Modulus and Poisson ratio of PVC solid rods were 1760 kg/m^3, 2.9 GPa and 0.4, respectively. We show that even a simplest geometry is capable of generating Dirac-like points at the center of the irreducible first Brillouin Zone (BZ) at several

frequencies with different geometrical parameters. Here we report two Dirac-like cones at the center of the BZ using a same lattice structure by modulating the geometric parameters of the resonator. Numerical results indicate that these Dirac-like cones are formed due to triple degeneracy which simultaneously contains a double and a single degenerate states when these degenerated bands show linear dispersions at $\vec{k} = 0$. Notably, a flat branch passes through each of these degenerate points with zero or approximately zero group velocity. Due to the symmetry breaking phenomena [23], we have shown that this flat branch does not transport any acoustic energy and exhibits spatial localization. Due to this non-transporting acoustical deafness behavior, this central flat band has been termed as 'deaf band' [24]. When a plane wave incident on the PnCs, this flat band shows antisymmetric acoustic mode shape with respect to the incident energy propagation direction. Deaf band is a consequence of the zero-effective density of the system and is only excited with the incidence of non-zero k-parallel components [23]. In this work, we present a predictive nature of accidental degeneracy yielding Dirac–like dispersions exploiting the properties of 'deaf band'. Here, we have portrayed the design of generation, modulation and control over Dirac-like cones. Also, the acoustic pressure field distributions are demonstrated over a range of Dirac frequencies[25]. Despite similar band structure at different Dirac-like points, here we demonstrate dissimilar behaviors at two Dirac frequencies as observed. Using the first Dirac frequency we have shown that the incident wave on the proposed PnCs is transported at an orthogonal direction as predicted by the dispersion mode shapes. Additionally, two 45° symmetric bent lines are observed which left a non-propagating zone insulated from the PnCs defects[26]. However, at the second Dirac frequency, a spiral wave guiding phenomenon is observed that repeats

convergence and divergence of acoustic pressure fields in the orthogonal directions with respect to the incident plane wave[27, 28]. Followed by the numerical simulations, an experimental setup was designed and realized for the verification of acoustic properties of the proposed structure. A good agreement was found between the numerical and experimental outcome.

This study has seven primary chapters. Following the first chapter which is the Introduction, in the second chapter, analytical derivation to find the dispersion curves for the periodic media mentioned above is presented. In the third chapter, we have proposed a predictive Dirac-like point modeling of resonator to predict the occurrence of triple degeneracy and dedicated to two Regions of Dirac-like cones in the dispersion curve. We present and explain the orthogonal wave transport phenomena at the Dirac-like frequencies in the PnCs, which are predictively identified. Here we have showed multiple Dirac-like point behavior under plane wave actuation condition. The fourth chapter is the about the experimental validation and study of chapter 3. The fifth chapter is regarding generation of dual-Dirac points by using angle orientation tuning. Tunable topological conduction has been proposed and studied in chapter 6. Finally, conclusion and future works have been presented in chapter 7.

CHAPTER 2

ANALYTICAL THEORY

It is reported that the plane wave expansion method in 3D periodic structure in solid-fluid media with spherical PnCs is not convenient [29-32] due to convergence issues with smaller number of expansions. However, with increasing computing facility using higher number of expansions one could lead to convergence with careful sorting of the eigen modes and proper definition of structural factor [33]. In this study, long cylindrical PVC rods arranged in air matrix are considered, where the wave modes propagated in x-y plane orthogonal to the axis of the cylinders (i.e. z-axis) are decoupled from the waves in the z-direction and the analysis remains 2D. Such conditions with plane wave expansion method was solved and proved to be accurate in Al/air [34] and PVC/air system [35, 36], by incorporating sufficiently large number of reciprocal space vectors. The study reported in Ref [35] with plane wave expansion method was thoroughly verified [16] using finite element method simulation. Analytical solution of wave dispersion in periodic structure formed by solid circular PnCs in air media was previously studied using plane wave expansion method [35], briefly reviewed herein. The governing differential equation of wave motion in any media can be written as

$$\sigma_{nl,l} + f_n = \rho \ddot{u_n} \qquad (1)$$

Utilizing standard index notations, we define $\sigma_{nl,l}$ as the derivative of the stresses with respect to the lth direction, f_n as the body force in the nth directions, ρ as the density

of the material and $\ddot{u_n}$ as the acceleration in the nth direction. In PVC-air setup, this will result in two governing differential equations.

Applying Bloch-Floquet condition [37] in reciprocal wave number space and adding $\vec{G}_1 = \frac{2\pi j}{D_1}$ and $\vec{G}_2 = \frac{2\pi m}{D_2}$ with the Eigen value wave number, we get the Bloch-Floquet displacement function as follows,

$$u_1(\mathbf{x}, t) = \sum_j \sum_m A_{jm} e^{i\mathbf{k}.\mathbf{x}} e^{i\mathbf{G}.\mathbf{x}} e^{-i\omega t} \quad (2)$$

$$u_2(\mathbf{x}, t) = \sum_j \sum_m B_{jm} e^{i\mathbf{k}.\mathbf{x}} e^{i\mathbf{G}.\mathbf{x}} e^{-i\omega t} \quad (3)$$

Where j and m are integers. Similarly, differentiating the displacement function twice with respect to time, the acceleration can be found as follows,

$$\ddot{u_1}(\mathbf{x}, t) = -\omega^2 \sum_j \sum_m A_{jm} e^{i(\mathbf{k}+\mathbf{G}).\mathbf{x}} e^{-i\omega t} \quad (4)$$

$$\ddot{u_2}(\mathbf{x}, t) = -\omega^2 \sum_j \sum_m B_{jm} e^{i(\mathbf{k}+\mathbf{G}).\mathbf{x}} e^{-i\omega t} \quad (5)$$

where j and m take numbers from -h to +h, where h is also an integer, D_i = a = lattice constant of the unit cell. The expression in Eq. (2) to Eq. (5) signifies summations over a range of values of j and m.

Stress function in Eq. (1) is the multiplication of the constitutive properties of the media and the strain function which can be further derived from the derivative of the displacement functions in Eq. (2) and (3). Here, the constitutive properties are assumed to be the function of space and expressed using Fourier coefficients, in the periodic media. Hence, applying the Fourier transform on the constitutive function and writing $C_{ts}(x)$in terms of C_{ts}^{pq} we get

$$C_{ts}(x) = \sum_{p=-h}^{h} \sum_{q=-h}^{h} C_{ts}^{pq} e^{i\left(\frac{2\pi p}{D_1} x_1 + \frac{2\pi q}{D_2} x_2\right)} = \sum\sum C_{ts}^{pq} e^{i\mathbf{G_{pq}}.\mathbf{x}} \quad (6)$$

Similarly, the derivative of the constitutive function with respect to space x_l can be written as follows,

$$\frac{\partial C_{ts}(x)}{\partial x_l} = (-1)^{l+1} \sum\sum iC_{ts}^{pq} \frac{2\pi(p(2-l)+q(1-l))}{D_l} e^{i\mathbf{G_{pq}}.\mathbf{x}} \quad (7)$$

Where, $C_{ts}^{pq} = \frac{1}{A_c} \int C_{ts}(x)\ e^{-i\mathbf{G_{pq}}.\mathbf{x}}$

And can be expressed as

$$C_{ts}^{pq} = \zeta_{air}\delta_{\mathbf{G_{pq}}0} + (\zeta_{PVC} - \zeta_{air})F(G_{pq}) \quad (8)$$

where, $\zeta_{air}\ or\ \zeta_{PVC}$ is the volume fraction of the respective constituent media, δ is Kronecker delta symbol, $F(G_{pq})$ is called the structural factor of the PVC in air, can be expressed as [33] $2fJ_1(G_{pq}r)/\mathrm{G_{pq}r}$, Where, J_1 is the Bessel function of the first kind, r is the radius of the PVC rods.

Substituting the Eq. (2) through Eq. (7) in to Eq. (1) we get two equations as follows,

$$\sum_j \sum_m \sum_p \sum_q \Bigg[A_{jm} C_{11}^{pq} e^{i(\mathbf{k}+\mathbf{G_{pq}}+\mathbf{G_{jm}}).\mathbf{x}} \left(k_1 + \frac{2\pi j}{D_1}\right)\left[-k_1 - \frac{2\pi j}{D_1} - \frac{2\pi p}{D_1}\right] +$$

$$\frac{1}{2} A_{jm} C_{66}^{pq} e^{i(\mathbf{k}+\mathbf{G_{pq}}+\mathbf{G_{jm}}).\mathbf{x}} \left(k_2 + \frac{2\pi m}{D_2}\right)\left[-k_2 - \frac{2\pi m}{D_2} - \frac{2\pi q}{D_2}\right] + B_{jm} C_{12}^{pq} e^{i(\mathbf{k}+\mathbf{G_{pq}}+\mathbf{G_{jm}}).\mathbf{x}} \left(k_2 +$$

$$\frac{2\pi m}{D_2}\right)\left[-k_1 - \frac{2\pi j}{D_1} - \frac{2\pi}{D_1}\right] + + \frac{1}{2} B_{jm} C_{66}^{pq} e^{i(\mathbf{k}+\mathbf{G_{pq}}+\mathbf{G_{jm}}).\mathbf{x}} \left(k_1 + \frac{2\pi j}{D_1}\right)\left[-k_2 - \frac{2\pi m}{D_2} - \frac{2\pi q}{D_2}\right]\Bigg] =$$

$$-\rho\omega^2 \sum_j \sum_m A_{jm} e^{i(\mathbf{k}+\mathbf{G}).\mathbf{x}} e^{-i\omega t} \quad (9)$$

$$\sum_j \sum_m \sum_p \sum_q\ A_{jm} C_{21}^{pq} e^{i(\mathbf{k}+\mathbf{G_{pq}}+\mathbf{G_{jm}}).\mathbf{x}} \left(k_1 + \frac{2\pi j}{D_1}\right)\left[-k_2 - \frac{2\pi m}{D_2} - \frac{2\pi q}{D_2}\right] +$$

$$+ \frac{1}{2} A_{jm} C_{66}^{pq} e^{i(\mathbf{k}+\mathbf{G_{pq}}+\mathbf{G_{jm}}).\mathbf{x}} \left(k_2 + \frac{2\pi m}{D_2}\right)\left[-k_1 - \frac{2\pi j}{D_1} - \frac{2\pi p}{D_1}\right] +$$

$$+ B_{jm} C_{22}^{pq} e^{i(\mathbf{k}+\mathbf{G_{pq}}+\mathbf{G_{jm}}).\mathbf{x}} \left(k_2 + \frac{2\pi m}{D_2}\right)\left[-k_2 - \frac{2\pi m}{D_2} - \frac{2\pi q}{D_2}\right] +$$

$$+\frac{1}{2}B_{jm}C_{66}^{pq}e^{i(\mathbf{k}+\mathbf{G_{pq}}+\mathbf{G_{jm}}).\mathbf{x}}\left(k_1+\frac{2\pi j}{D_1}\right)\left[-k_1-\frac{2\pi}{D_1}-\frac{2\pi p}{D_1}\right]=$$

$$-\rho\omega^2\sum_j\sum_m A_{jm}e^{i(\mathbf{k}+\mathbf{G}).\mathbf{x}}e^{-i\omega t} \qquad (10)$$

After mathematical simplification Eq. (9) and Eq. (10) result an eigen value problem and the size of the matrix depends on the number of terms used in the summation. The eigen value of the proposed system can be further solved for the wave dispersion relationship. However, adopting this Plane Wave Expansion (PWE) approach may result in convergence issue at some frequency points in solid-fluid mixed media[29-32, 38]. To circumvent this problem, finite element method can be utilized with acceptable accuracy. In this article, the band structure shown in Figure 1 has been constructed using COMSOL Multiphysics 4.3.

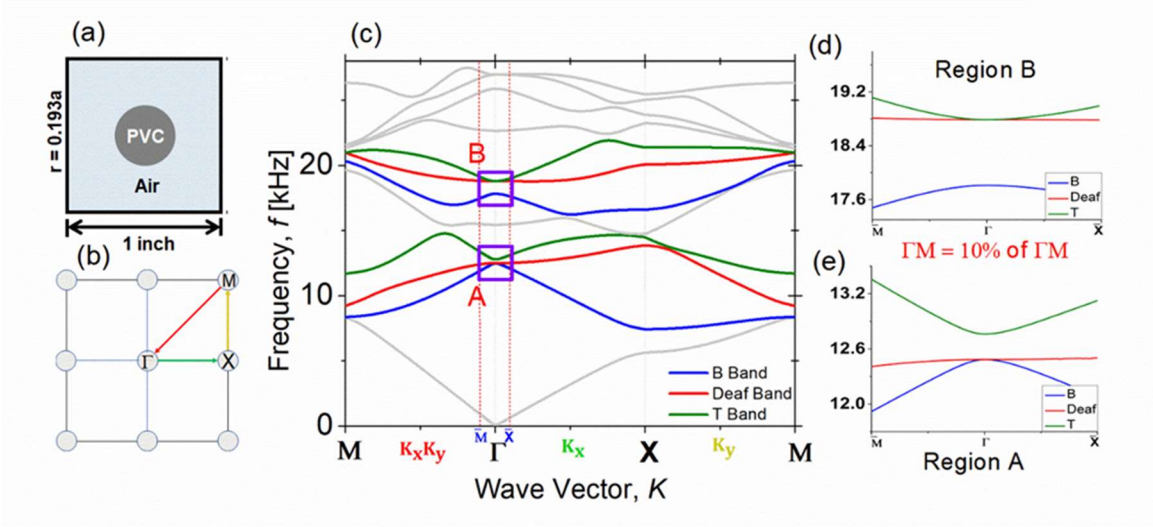

Figure 2.1: (a) A single lattice of a = 1inch and r=0.193a, (b) Brillouin Zone depicting wave vector direction, (c) Band structure for the unit cell, (d) Band structure of the unit cell, showing 'Region A' and 'Region B', with two possible Dirac-like degenerated point, (b) and (c) Zoomed in view of 'Region A' and 'Region B'.

CHAPTER 3

DEAF BAND BASED PREDICTIVE MODULATION

3.1 Background

Unlike systematic essential degeneracies, accidental degeneracy depends on the geometrical parameters of the system. The term 'accidental' indicates two eigen functions belonging to the bases of two different irreducible representations that correspond to the same level of energy. Although geometrically symmetric, in case of accidental degeneracy, the obvious equivalent configuration of the irreducible representations is not always guaranteed. Hence, accidental degeneracy and the generation of the double or triple degeneracy occurs at certain specific configurations which are still under active research area. In this article, we have proposed a 'deaf band' based nearly predictive nature of the accidental degeneracies at the Dirac-like points, if the 'deaf bands' are identified from the dispersion behavior utilizing an arbitrary geometric structure.

3.2 Deaf Band based modulation

Determination of dispersion behavior is the first step of prediction methodology. First the possible frequency regions at Γ (where the wave vector, $\vec{k} = 0$) point are identified based on the 'deaf' bands. From the frequency-wavenumber plot for PnCs (*r = 0.193a, 11.7% volume fraction)*, the trend to generate probable Dirac-like points at different frequencies are determined. In this study, we identified two probable points near ~12.5 kHz and ~18.5 kHz where the possibilities of getting Dirac-like phenomenon was obvious

because of the existence of two double degenerate states. We named these regions as 'Region A' and 'Region B'. More specifically, 'Region A' was within ~11.7 – 13.5 kHz band and 'Region B' was within ~17.5 – 19.7 kHz frequency band, as shown in Figure 2.1d & e. Three bands in 'Region A' and 'Region B' are named 'T' and 'B' for the top and bottom bands, respectively with respect to the 'deaf' band. The acoustic pressure mode shapes with the deformation of the PVC rods are presented in Figure 3.1a for the 'T', 'B' and the 'deaf' bands. Investigating the air pressure wave modes of 'T', 'B' and the 'deaf' band we clearly see that 'T' and 'B' (two orthogonal quadrupole mode) has proper symmetry that can be excited by an incident plane wave along ΓX [100] and XM [010] direction, whereas the 'deaf' band mode (dipolar) is antisymmetric, with almost zero group velocity along the incident wave direction. The deformation pattern of the PVC rods from the height expression (Figure 3.1b1 & b2**)** for the 'deaf' band is dominated by the deformation of the rods along the incident direction with a very small translation (Figure 3.1b2) along the XM direction, which is orthogonal to the Γ*X*. Whereas, for 'T' and the 'B' band the PVC rods has quadrupole deformation with reduced radius but without translation along any direction (Figure 3.1b1**)**. Thus the 'deaf' band cannot be excited by the normal-incident plane wave due to the asymmetry. Moreover, superposition of 'T' and 'B' band air pressure near the possible Dirac frequency may overlaps to cause reduced transmission of the incident wave. A sample domain of 5 x 4 block of PnCs before tuning (i.e. with r = *0.193a, 11.7% volume fraction*) is investigated numerically within the band 10 kHz – 14 kHz. Although the zero-group velocity band starts at ~12.55 kHz the transmission started to drop to below 50% close to ~12.0 kHz. Transmission further dropped due to the asymmetric 'deaf' band although there is no band gap along the ΓX [100] direction. Here

we will call the nearly zero group velocity band as the ‘deaf’ band as previously called in Ref [23, 39, 40].

From Figure 2.1, it is intuitive that if the band ‘T’ in ‘Region A’ is moved downward and the band ‘B’ in ‘Region B’ is moved upward, triple degeneracies are possible. Hence, optimizing or tuning geometric parameter could lead to the dispersion modes aiming to generate accidental triple degeneracy. Although it was shown that this antisymmetric mode cannot be excited [23, 31] in the incident direction, we found that after

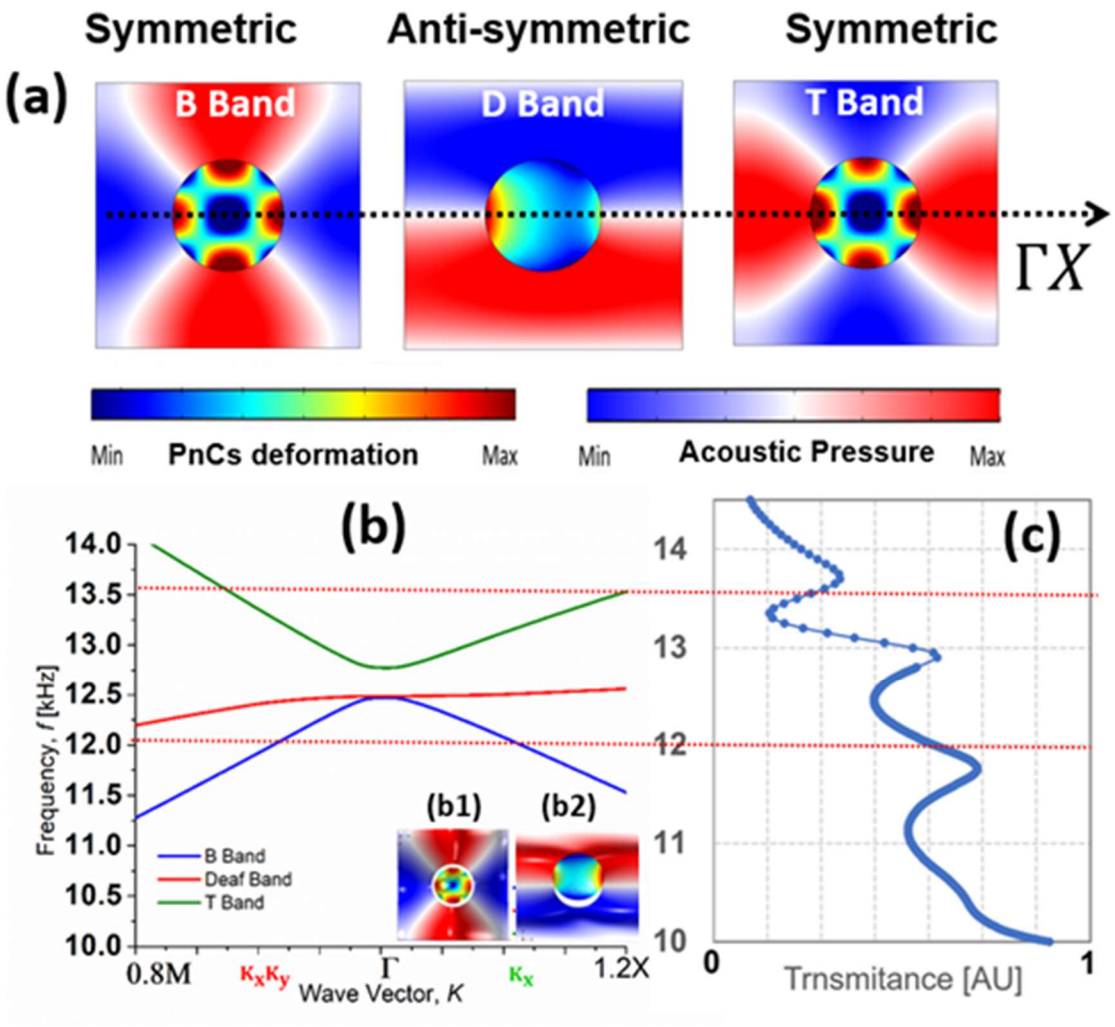

Figure 3.1: The band structure of the region A, with the transmission given at the right for frequencies from 11.5 – 13.5 kHz. It can be seen that the wa at deaf band frequency, due to having antisymmetric mode shape given.

tuning at Dirac-like cone frequency, due to the triple degenerate state, they starts to propagate along the orthogonal direction keeping the antisymmetric pattern along the incident direction, a sharp 45° bent line to the incident wave and the Berry-phase equal to zero [41] at the Dirac frequency. A close observation of 'Region A' reveals that the band 'B' and the deaf band are already merged, however, the band 'T' maintains an apparent band gap with the deaf band which is shown in Figure 2.1e. An apparent solution could be to lower down this 'T' band with respect to frequency while unaltering the position of the deaf band which would generate a Dirac-like point. Now in step three, the geometric

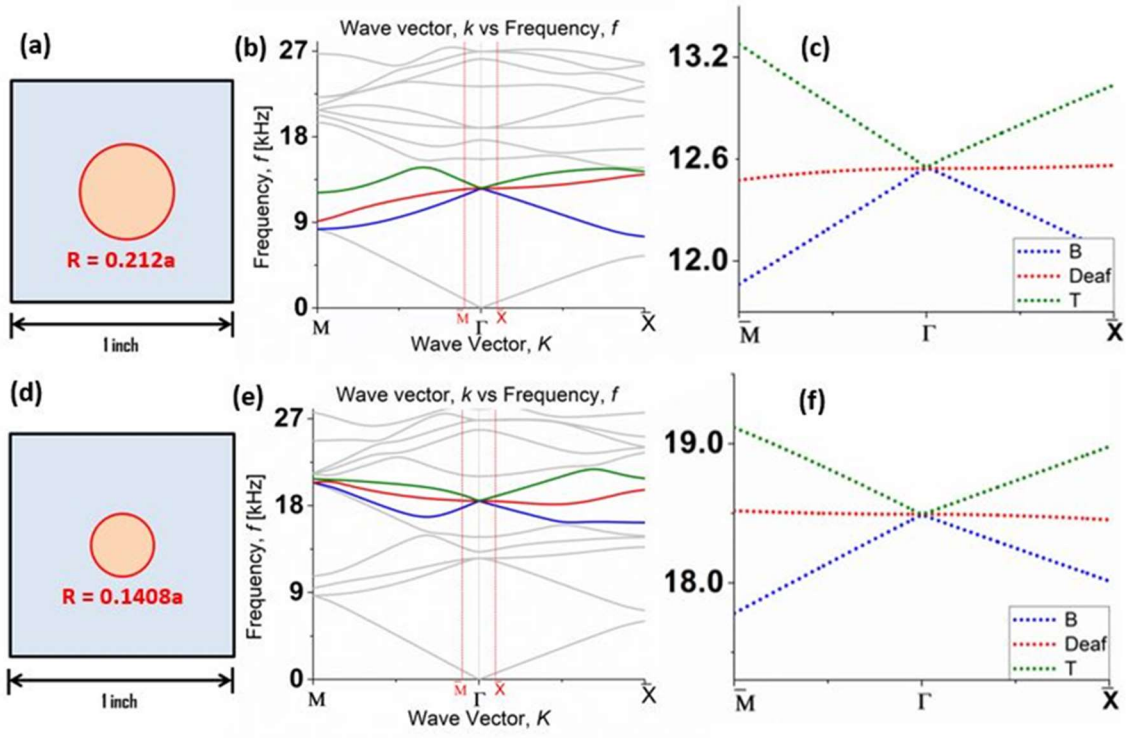

Figure 3.2: Accidental degeneracy at 'Region A' and "Region B' (a) A unit cell for region 'A' of PnCs of radius, r = 0.212a in air matrix, (b) Dispersion relation for region 'A' after increasing the radius, r = 0.193a to r = 0.212a where the T band lowered down with respect to Deaf band and having an accidental degeneracy. for the frequency, f = 12.551 kHz c) Zoomed in view of the 'Region A' Dirac-like point, d) A unit cell for region 'B' of PnCs of radius, r = 0.1408a in air matrix, (e) Dispersion relation after decreasing the radius, r = 0.193a to r = ~0.1408a where the B band moved upward with respect to Deaf band and having an accidental degeneracy. for the frequency, ω = 18.512 kHz. f) Zoomed in view of the 'Region B' Dirac-like point.

parameter, radii in this case, has been optimized and increased from r = 0.193a to r = 0.212a of the resonators. This results in significant alteration of the 'T' band in terms of frequency position while keeping approximate (~+0.08%) fixed position of the 'deaf band' and the 'B' band frequency at Γ point. The dispersion of the 'T' band altered to a local linear dispersion. Two branches of linear dispersion intersect at a triply degenerate point at $\vec{k}$=0, forming a Dirac-like cone at f = ~12.551 kHz. Triple degenerated Dirac-like point at 'Region A' has been shown in Figure 3.2c.

Similar approach was adopted for 'Region B' (Figure 2.1d), the band 'T' and the 'deaf band' had an intersection at Γ point forming a local band gap with the band 'B'. Unlike 'Region A', since the gap was between the band 'B' and the double degenerated state, through optimization, the radii of the PVC rods were decreased from r = 0.193a to r = 0.1408a. This resulted in significant alteration of the dispersion of the band 'B' in terms of frequency position and formed local linear dispersion which intersected the 'deaf band'. While the frequency position of band 'B' has been altered, the 'deaf band' and 'T' band frequencies were very close to the frequencies they were originally detected at the Γ point with ~1% perturbation. This created another Dirac-like point at a frequency of f = ~18.512 kHz. Triple degenerated Dirac-like point at 'Region B' has been shown in Figure 3.2e. Notably, in both cases, it was evident that the 'deaf band' played an important role in pivoting the triple degeneracy. While an insignificant change (< ~0.08% in Region A and < ~1% in Region B) of 'deaf band' Dirac frequency at Γ point was observed, it rather helped 'T' and 'B' band to modulate predictively by altering the radii of the PnCs. Thus, if the radii of the resonators increased, the Γ point frequency of the 'T' band decreased, whereas if the radii of the resonators decreased, the Γ point frequency of the 'B' band

increased. All these alterations of frequency positions were relative to the Γ point frequencies of the 'deaf band'.

3.3 Numerical Simulations

To prove whether the triple degenerated Dirac-like points based on 'deaf bands' are exhibiting the Dirac cone behavior, we simulated PnCs made of PVC rods in two configurations – one with r = 0.211a and the other with r = 0.1408a as shown in Figure 3.2. To demonstrate the wave transmission behavior, a frequency domain study was performed near the Dirac frequencies to obtain the acoustic pressure field distributions using

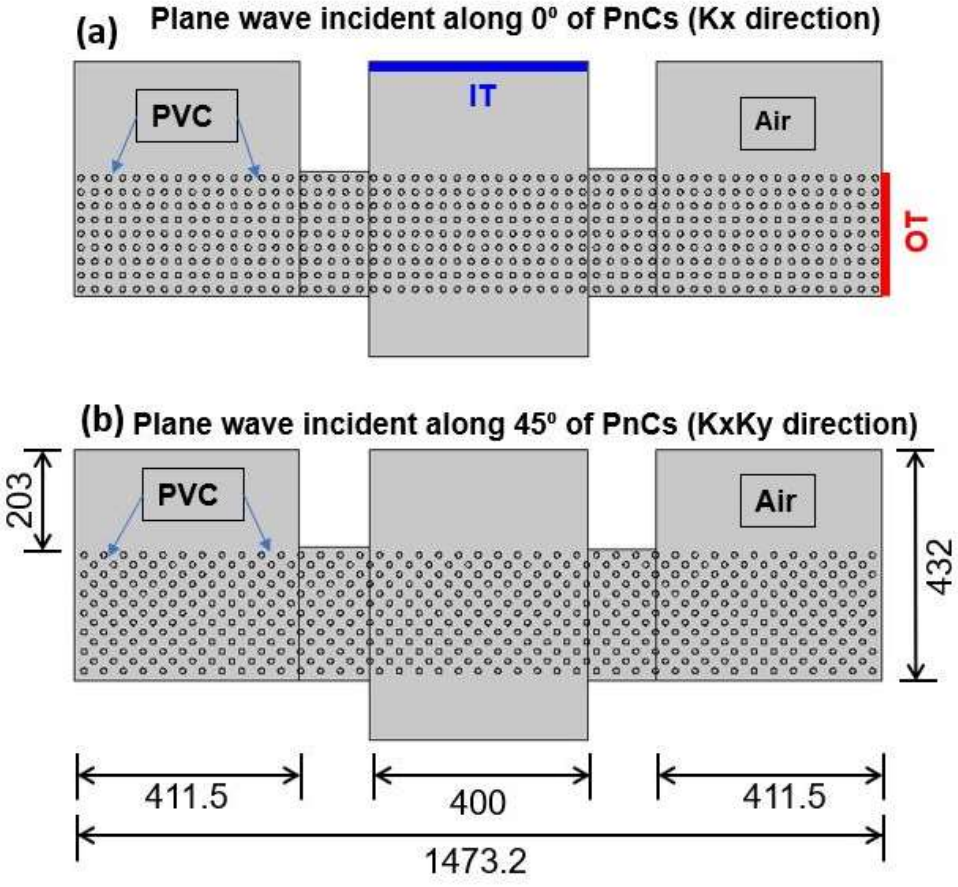

Figure 3.3: Model for the numerical experiments, and analysis for plane wave propagation through PVC PnCs having incident at 0 Degree and 45 Degree angle, respectively (ΓX and MΓ direction, respectively)

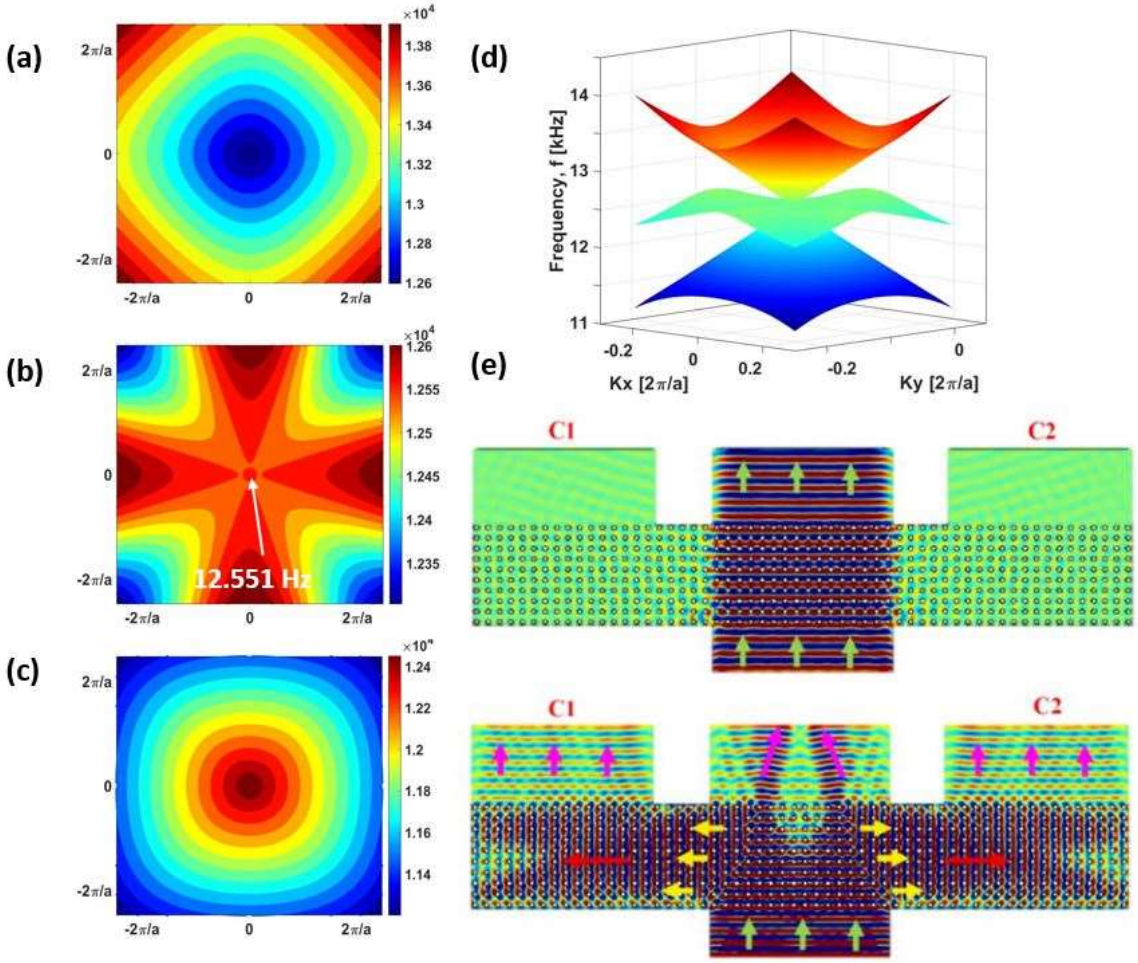

Figure 3.4: (a), (b) and (c) depicts the Equi-frequency surface (EFS) for T band, Deaf band and B band respectively for region A. Here, the frequency contour for Dirac-like frequency looks circular (in (b)), by proving the isometric behavior of acoustic wave at Dirac frequency. Whereas, all the other frequencies, the contours are not fully circular anisotropic). (d) An Equi-frequency Contour (EFC) of region A, (E) the absolute acoustic pressure field for plane wave generated in ΓX direction for frequencies of f = 10kHz and f = 12.551 kHz respectively. Here we can see that, while the plane wave was propagating through the PnCs at f = ~10kH without changing any direction, the wave has been transported orthogonally in a converging – diverging pattern when propagated at the Dirac like frequency of f = ~12.551 kHz After reaching the end of the tunnel, the wave has again turned orthogonally keeping the plane wave pattern undisturbed along C1 and C2 channels.

commercially available COMSOL Multiphysics simulation software. A rectangular arrangement consisting of 57 x 10 solid PVC cylinders in air media were designed for the numerical simulations. The actuation of the PnCs arrangement was performed by a guided

plane wave source located at a distance of 0.112 m from the Air-PVC interface. As shown in Figure 3.3a and 3.3b, two different angles of incidence of the actuating plane waves on the PnCs were studied - (a) along 0° (ΓX direction) and (b) along 45° (MΓ direction), respectively. A plane wave radiation boundary condition was assumed at all the boundaries in these numerical simulations. To demonstrate the behaviors such as orthogonal wave transportation and negative refraction at Dirac-like frequency points, two channels namely C1 and C2 were routed, center lines of these routes were ~0.533 m away from the central line of the central channel as shown in Figure 3.3.

Although both 'Region A' and 'Region B' demonstrated the orthogonal wave transport, which is an inevitable feature at Dirac frequency, each region has its own unique features that can be explained through the respective wave dispersion behavior. In this article, features of the Regions A are discussed exclusively.

3.3.1 Region A: Proof and Features of Direct-Like Cone

Orthogonality in plane wave propagation was previously reported by the researchers [4, 7] at Dirac-point frequency, where the Dirac points exist at the boundary (X or M points) of the Brillouin zone of PnCs. However, here we report the orthogonal wave transportation at the Dirac-like frequencies at the Γ point, where the wave vector, $\vec{k}=0$. At r = 0.212a of the PVC cylinder, a Dirac-like point is generated at the center of the Brillouin zone with a Dirac frequency of ~12.511 kHz, as shown in the dispersion curves in Figure 3.2 c.

3.3.1.1 Orthogonal Wave Transportation - Propagation along $\boldsymbol{\Gamma X}$

Wave guiding, and propagation pattern was studied inside and outside the PnC arrangement (Figure 3.4) near the estimated Dirac frequency. Figure 3.4 (e) shows the

acoustical pressure field distribution at a frequency at 10 kHz, slightly below the Dirac frequency, which is also similar above the Dirac frequency. This is consistent with the phenomena reported in Ref. [3, 6]. While the plane wave propagates in the direction of actuation without any distortion at a frequency slightly below or above the Dirac frequency, a drastic orthogonal wave transport (wave takes a 90° turn) was observed at Dirac frequency shown in Figure 3.4e. At the Dirac frequency only, a little acoustical energy propagates in the direction of actuation creating a partial band-gap like situation. As wave propagates inside the orthogonal transport became prominent leaving a 45° diversion line as shown in Figure 3.4e. However, wave again take 90^{o} turn towards the original wave propagation direction in C1 and C2 channels leaving leaky plane waves, a result of negative refraction phenomena. From the acoustic transmission behavior through the cylinders generated numerically, an attenuation peak or a transmission loss along the incident plane wave direction (ΓX) is detected at the Dirac-like point frequency. This phenomenon happens to be due to the presence of the Deaf band, which can be explained by the particular symmetry of the states. have plotted Acoustic pressure eigenmode shapes of B band and Deaf band near Γ point of the first BZ for $r = 0.193a$. From the Acoustic pressure field mode pattern, of Fig 1, we see that B band has proper symmetry that can be excited by an incident plane wave along ΓX direction or [010] direction, whereas the Deaf band mode pattern planes travel perpendicular to the incident wave direction, having equal phase like B band. Hence, the Deaf band, being flat and having almost zero group velocity, cannot

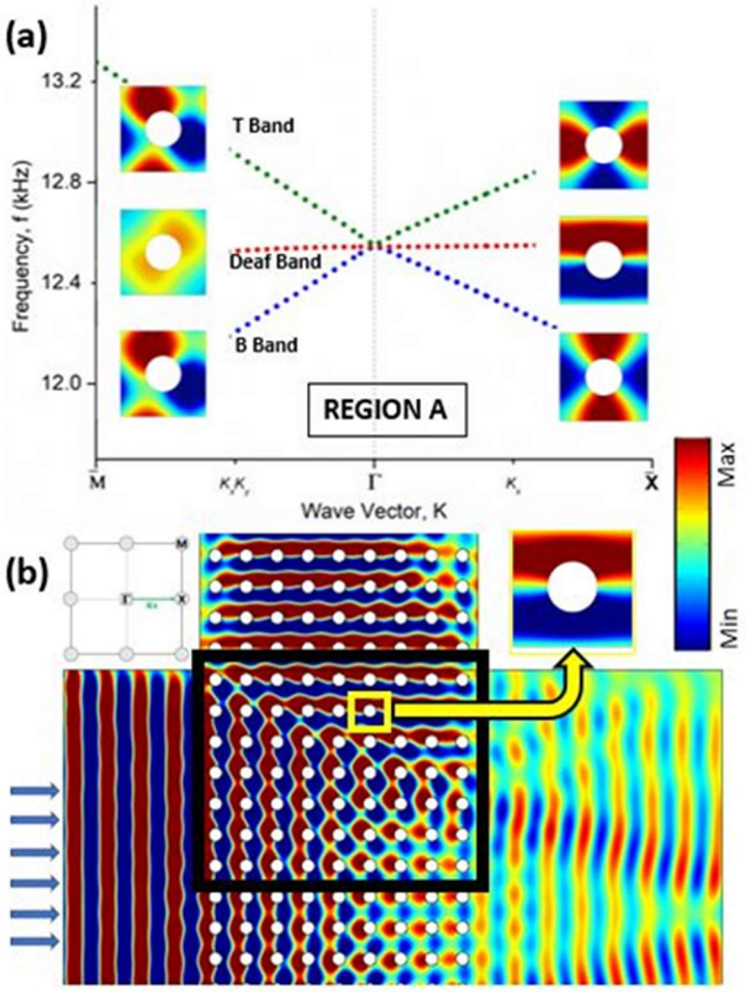

Figure 3.5: (a) Band structure with mode shapes of T, deaf and B band for ΓX direction, (b) depicting the resemblance of the acoustic pressure distribution during orthogonal transportation with the ΓX deaf band mode shape, having the direction of excitation being ΓX (given in inset

exhibiting strong spatial localization and cannot be excited depending on mode symmetry compared to the source. Now, the term 'deaf band' has been reported several times by many authors, where we have found couple of genres of them. Initially, the band that acts indifferent upon planar wave front excitation has been referred as a symmetry forbidden band due to symmetry breaking. In this case, the group velocity of the band is not necessarily zero. Sanchez-Perez et al announced the term 'deaf band; for the first time,

showing a positively sloped band possessing wave attenuation property due to symmetry with incident planar wave. Whereas the second genre has been reported where the deaf band is flat with respect to wave vector i.e. deaf band possess zero or very small group velocity. The deaf band we are proposing here falls in the second genre where the transmission of incident planar wave attenuates due to symmetry breaking phenomena. [23, 39, 40, 42, 43]

Next the reason for this behavior is explained using the local dispersion of the degenerated mode shapes at Γ point (Figure 3.5). The mode shapes here are the total absolute acoustic pressure mode shapes. 'T' band and the 'B' band mode shapes are quadrupolar modes, orthogonal to each other, however, the 'deaf band' mode is a dipolar mode. Hence, the T band and the B band nullifies each other, keeping the deaf band dipolar mode to dominate the wave propagation in the PnCs. Now, if we look at the wave transmission behavior from the acoustic pressure field at Dirac-like cone (Fig 3.5b), to keep the dominant dipolar mode alive a 45^{O} bent line was inevitable which carries over the plane wave orthogonally.

3.3.1.2 Formation of 'No Zone' - Propagation along ΓX

Fig. 3.6a & b shows the close view of the acoustical wave field pattern, when the incident plane waves transported orthogonally inside the PnCs leaving two 45° bent lines. As the acoustic energy diverts along these 45° bent lines, no or little amount of energy is left to divert at the intersection of these bent lines leaving some of the unit cells unaffected by the incoming waves. The region of PnCs where no acoustic energy is available at or near Dirac frequency is referred 'No Zone' in this article.

The formation of ‘No Zone’ starts from ~12.48 kHz, as shown in Figure 8, and the area of the ‘No Zone’ continues to increase as the frequency increases. At ~12.52 kHz, which is close to the Dirac frequency, where the largest number of unit cells were unaffected and hence the largest area of the ‘No Zone’ becomes prominent.

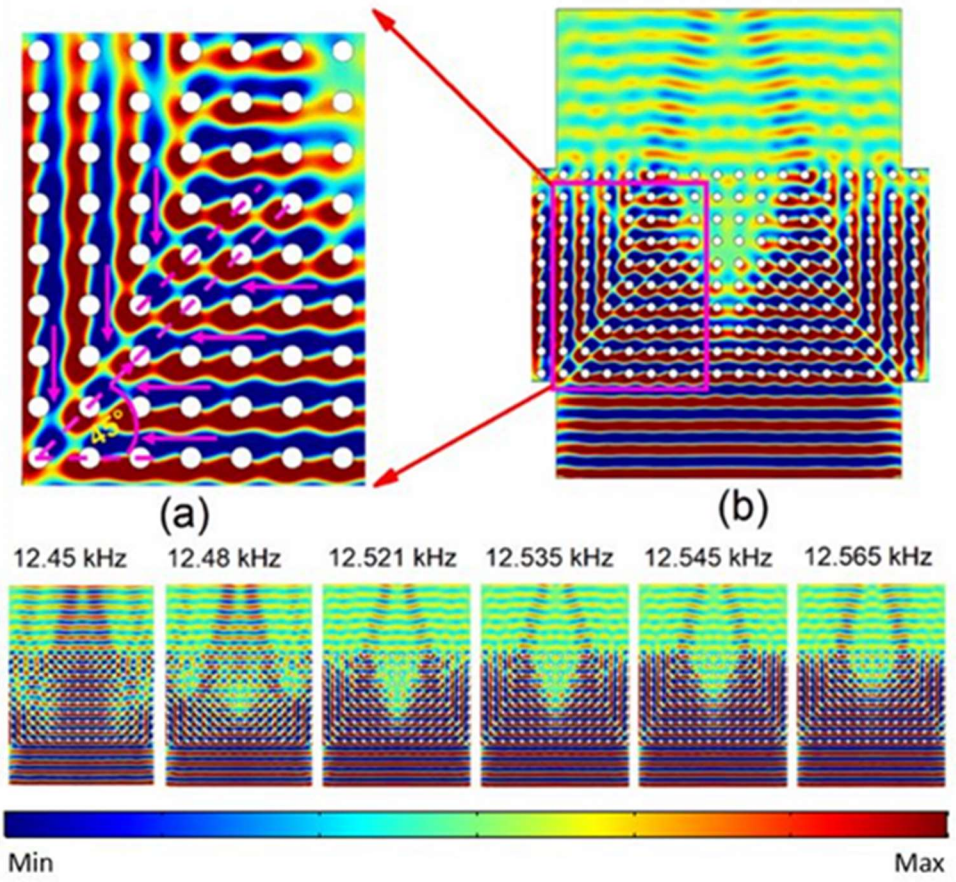

Figure 3.6: (a) The bent line where the plane wave deviates orthogonally maintaining a 45^{O} bent line (marked by pink dotted lines), (b) The zoomed-out region, showing a 'No Zone' at the verge of 2 bent lines, making a small region untouched by the plane waves, (c) The gradual formation of the ‘No Zone’ with the increasing frequency towards the Dirac-like frequency of Region A. It is to be noted that, the largest ‘No zone’ was identified at the actuated frequency of f =~12.521 kHz.

3.3.1.3 Acoustic Cloaking - Propagation along ΓX

Since the ‘No Zone’ is fully unaffected by the influence of incoming or outgoing acoustical energy, presence or absence of any object placed in this area can be hardly

identified. To concrete this claim, eight PVC cylinders located in a rectangular fashion at the center of the 'No Zone' were removed and plane waves were excited at 10 kHz, 12.535 kHz and 14 kHz, respectively. Figure 3.7 shows that, at Dirac frequency, absence of acoustic energy at the center of the 'No Zone' has no effect on the wave field, which is affected below or above the Dirac frequency. This phenomenon has the potential for the application in acoustic clocking.

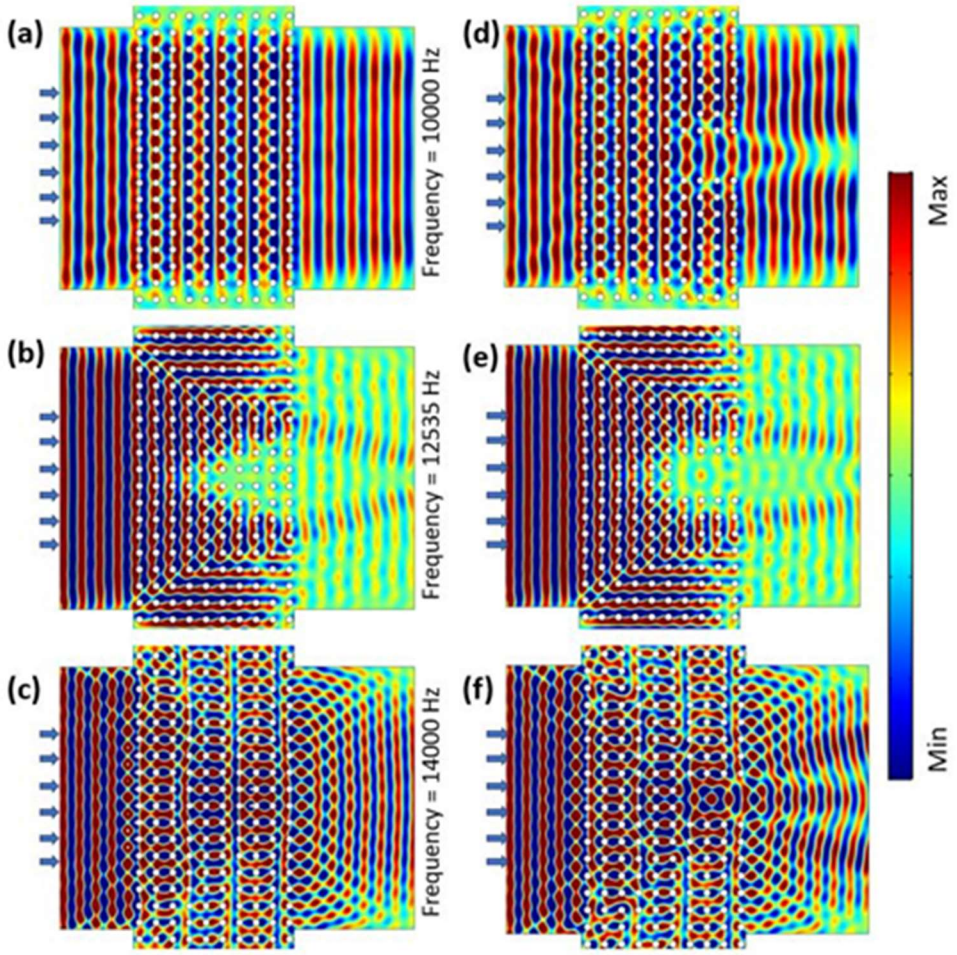

Figure 3.7: Acoustic cloaking phenomena was observed in (a), (b) and (c), depicting the acoustic pressure field and the wave transportation at frequencies of ~10, ~12.535 and ~14 kHz, respectively shows that the 'No Zone' is evident at f=~12.535 kHz. Now, after removing the PVC PnCs in that particular No zone field, we achieved similar phenomenon as shown in Fig. 8c.

3.3.1.4 Orthogonal Wave Transportation - Propagation along MΓ

Waves were actuated in the MΓ direction i.e. along the 45^{O} (numerical setup shown in Fig 3.3b with respect to the PVC PnCs orientation sweeping the frequency between 10 kHz and 13 kHz. Actuating the bottom boundary shown in Fig 3.8a-d, we see that the plane wave traveled along the actuation direction below the Dirac-like frequency, f = 10kHz (Figure 3.8a). With increasing frequency from the 'Region A' Dirac-like point, the wave starts to propagate orthogonally. Similar phenomena reported in section 3.3.1.1, near the entrance of the C1 and C2 (tip of red lines), the orthogonal wave again transported orthogonally towards the C1 and C2 channels leaving the leaky plane waves at f=~12.225 kHz (Figure 3.8b). At f = ~12.443 kHz (Figure 3.8c) and ~12.50 kHz (Figure 3.8d), the orthogonally transported waves have different behavior compared to section 3.3.1.1. Here waves get divided in to two tracks and made a hollow lobe to facilitate acoustic cloaking and created a wave vortex (or acoustic self-looping) with imaginary sources in the C1 and C2 channels.

Reason for such behavior can be explained using the local dispersion of the degenerated mode shapes at the Dirac frequency along the MΓ and ΓX direction. As discussed in section 3.3.1.1 with Fig. 3.5(a) the 'deaf band' mode is the dominant mode shape at the Dirac frequency along the ΓX direction which is along the 45^{O} compared to the MΓ direction. But the deaf band mode is weaker in magnitude (Figure 3.5a) compared to the T and B band mode shapes along the MΓ direction. This unique combination helps the wave to take a 135^{O} bent (Figure 3.8e) which is a local orthogonal direction along the ΓX.

However, due to the further weaker deaf bands along the MΓ direction wave reveals to take another local 45^{O} bent to keep the dominant deaf band mode shape along the ΓX direction, leaving the weaker MΓ deaf band mode shape at the boundaries (Figure 3.8g). This hindrance continues, and the travelling wave rotated back to the entry point, creating a wave vortex, we call self-looping at the Dirac frequency leaving a small 'No Zone', where the divergence of the acoustic displacement field is zero.

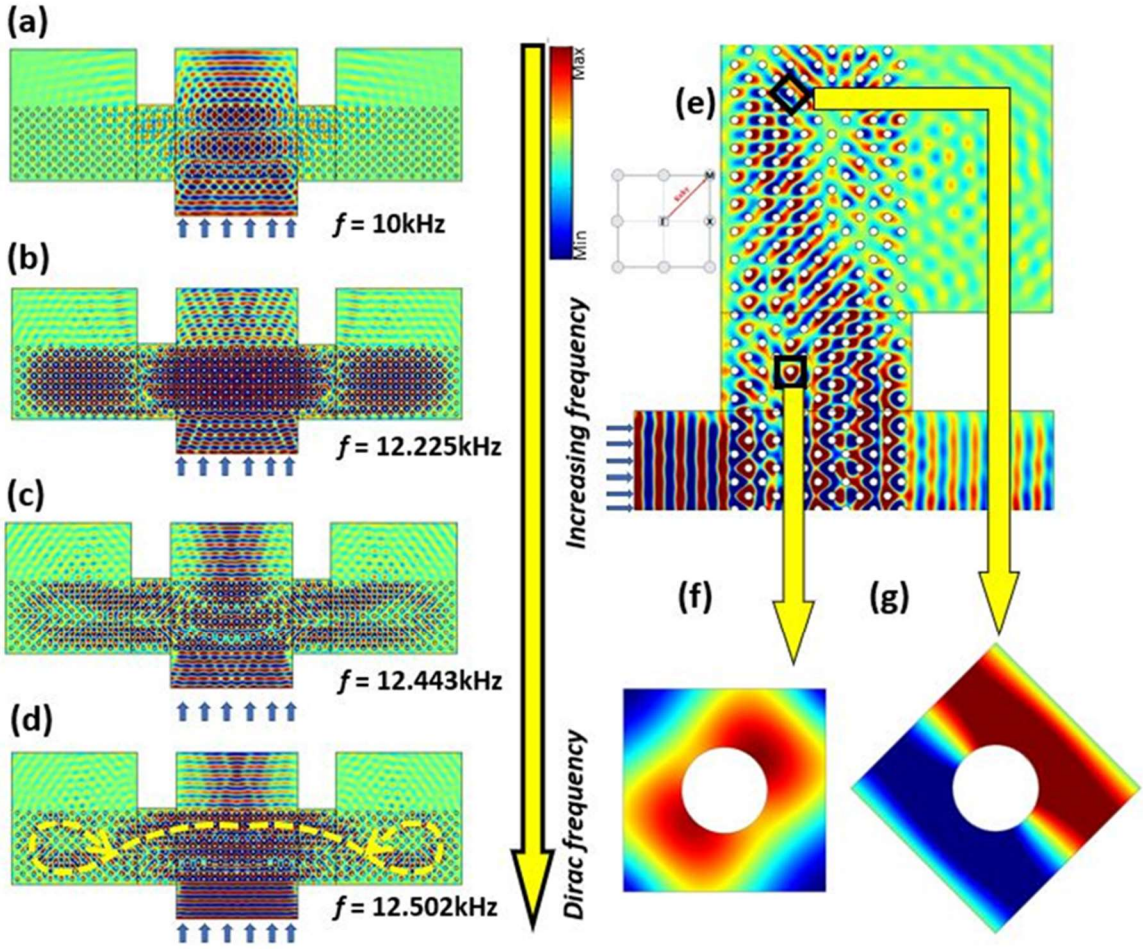

Figure 3.8: Plane wave transportation actuated at MΓ direction with respect to the PnCs arrangement for different frequencies. The orthogonal wave transport was observed at the frequencies around and at Dirac-like point. He we showed acoustic pressure field of wave actuated at (a) 10 kHz, (b) 12.225 kHz, (c) 12.443 kHz and (d) 12.502 kHz

3.3.2 Region B: Proof and Features of Direct-Like Cone

Similar phenomenon has been observed in the case of region-B too. The most interesting phenomenon starts emerging at the frequency of ~18.46 kHz (Which is very near (0.44%) to the Dirac-like frequency), when the orthogonally transported wave fronts form a converging-diverging phenomenon inside the periodic crystals. After increasing the column number of the PVC PnCs, we have confirmed that the convergent-divergent phenomenon keeps unchanged throughout the periodic materials. In Figure 3.9d-h, wave getting converged at a focal point and travelling in a spiral manner, inside the PnCs is observed. Interestingly, the plane wave that has been actuated in Kx direction, keeps propagating through the PnCs and after leaving the last row of PnC, maintain the plain wave-front pattern. In Fig 3.10, the plane wave front has been excited in MΓ direction, and a similar phenomenon has been observed.

3.3.2.1 Orthogonal Wave Transportation - Propagation along ΓX

Wave guiding, and propagation pattern was studied inside and outside of the PnC arrangement (Figure 3.9d). The bottom boundary was excited with a normal displacement in ΓX direction, for a range of frequencies sweeping around the Dirac-like frequency ~18.512 kHz. Figure 4d to h shows the acoustical pressure field distribution at frequencies from 18.119 – 18.512 kHz, and many propagation patterns are observed. Here, like region A, the plane wave starts travelling orthogonally before reaching the Dirac-like frequency, in Figure 3.9d. At f = 18.196 kHz, wave travels both in the actuation direction and in orthogonal direction. It is clearly observed that at the interface (the first row of PnCs) of the wave guide the plane waves remained plane. However, as propagated inside, the wave

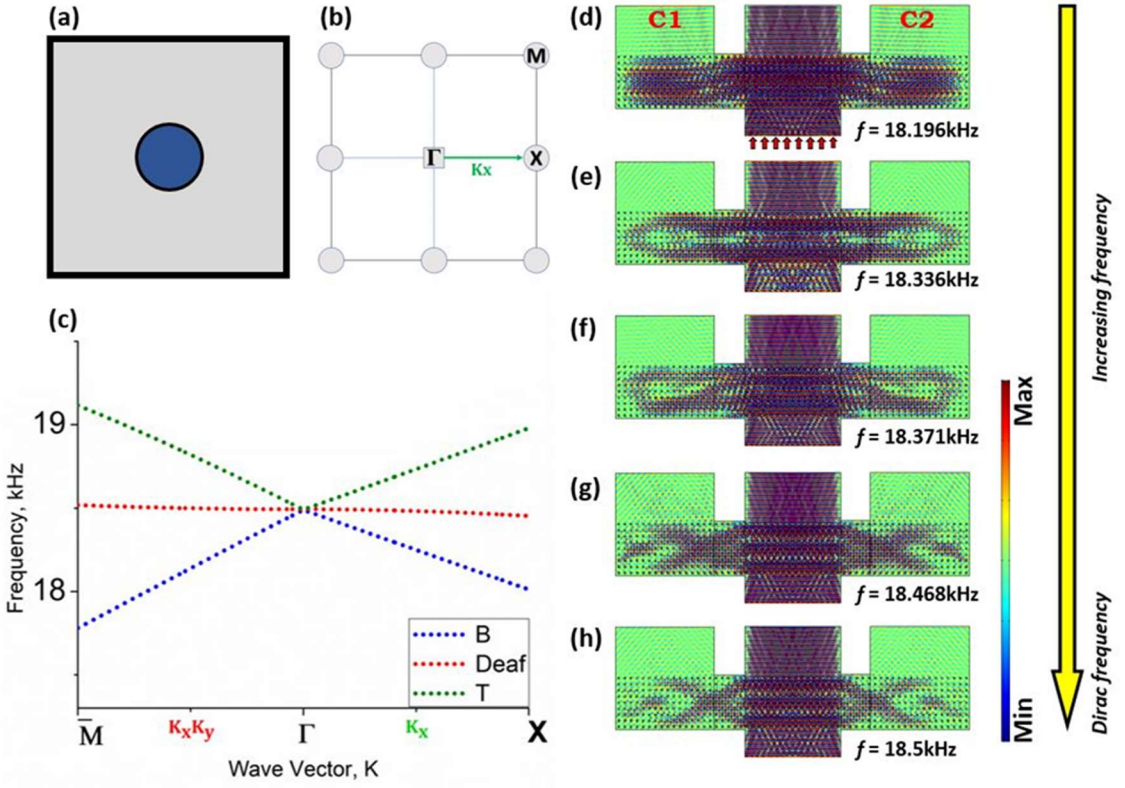

Figure 3.9: The unit cell of PnCs, (b) The first Brillouin zone structure, showing ΓX direction of wave vectors (c) The band structure showing Dirac-like point degenerated at f =~18.512 kHz at 'Region B', (d) to (h) the absolute acoustic pressure field for plane wave generated in ΓX direction for frequencies of f = ~18.196 kHz,18.336 kHz, 18.371 kHz, 18.468 kHz and 18.5 kHz respectively. Here we can see that, the wave has been transported orthogonally in a converging – diverging pattern when propagated at the Dirac like frequency of f = ~18.512 kHz

interacted with the further rows of PnCs and orthogonal transport of the wave became prominent. However, near the entrance of the C1 and C2, wave again transported orthogonally towards C1 and C2 channels leaving leaky plane waves, which is similar to a negative refraction phenomenon.

After increasing the actuation frequency towards Dirac-like frequency, at f = 18.336 kHz, the wave gets split into two beams, creating a non-affected PnC region at the center, shown in Figure 3.9e. The wave tends to reflect at the boundary after bouncing back towards the center of the PnC set, which is similar to a feedback phenomenon. The

orthogonally wave being split, keep changing the propagation pattern with the increasing frequency, like shown in Figure 3.9f. At f = 18.371 kHz, wave reflecting phenomenon at the two ends boundaries remains, but a unlike Figure 3.9e, a separate wave beam forms at the middle, merging the lower beam at an angle. The most interesting phenomenon starts emerging at the frequency of ~18.46 kHz, when the orthogonally transported wave fronts form a converging-diverging phenomenon inside the periodic crystals. After increasing the column number of the PVC PnCs, we have confirmed that the convergent-divergent phenomenon keeps unchanged throughout the periodic materials. In Figure 3.9g, wave getting converged at a focal point and travelling in a spiral manner, inside the PnCs is observed. Interestingly, the plane wave that has been actuated in Kx direction, keeps propagating through the PnCs and after leaving the last row of PnC, maintain the plain wave-front pattern. Finally, at the Dirac-like frequency, at f = 18.551 kHz, the orthogonal spiral propagation is distinct and obvious from Figure 3.9h. However, with the increase of the frequency towards Dirac-like frequency, the wave converging focal length inside the PnCs keep reducing and the wave beams that are being converged gets narrowed. That means, if we think of the wave beams as bands of two acoustic spectrums converging at a focal point, then the focal point can be modulated with increasing and decreasing operating frequency near Dirac point. Hence, channelized wave transport is realized herein, suitable for designing tailored wave propagation at and around Dirac-like frequency.

3.3.2.2 Orthogonal Wave Transportation - Propagation along MΓ

Now, similarly, we investigated the wave transportation behavior sweeping the frequency range around the Dirac-like frequency of region B. This time, waves were actuated in the MΓ direction i.e. along 45^{o} incident angle with respect to the PVC PnCs

orientation. We used the numerical setup shown in Fig 3.3b, where we have arranged the periodic crystals in such way that the actuation plane wave-front interact with the PnCs along MΓ direction (at 45^{o} angle). Like section 3.3.1.4, we actuated the bottom boundary of Figure 3.10d.

Actuating the bottom boundary shown in Figure 3.10d, we see that the plane wave traveled along the actuation direction below the Dirac-like frequency, f = 18.411 kHz similar to section 3.3.1.4. With the increasing frequency at the 'Region B' Dirac-like point, the wave starts to propagate orthogonally. Like reported before in section 3.3.1.4, near the entrance of the C1 and C2, wave again transported orthogonally towards C1 and C2 channels leaving leaky plane waves. In this case, actuating plane wave passes through the PnCs and keep propagating along the actuation direction (MΓ direction), leaving a small amount to travel orthogonally. With increase of frequency towards the Dirac-like frequency, like section 3.3.1.4, the orthogonal wave transportation dominates inside the PnCs, having a shift of the wave-front beam in any of the one direction.

In case of f = 18.464 kHz, from Figure 3.10e, the shift is away from the actuation direction, at the verge of the last rows towards the C1 and C2 channels. Interestingly, a distinct pair of acoustic beams are observed at the center channel, leaving the PnCs, along the actuation direction, which gets decayed afterwards with the increase of frequency. When the frequency reaches f = 18.479 kHz, the wave-front beam shifts down, towards the actuation direction boundary, shown in Figure 3.9f. Hence, the wave transportation pattern keeps changing inside the PnCs from f = 18.464 kHz to f = 18.479 kHz, where the wave switches

it's converging tendency from one side of PnC to the other side. Plane wave get converged, like section 3.3.1.4, at a frequency, very close to the Dirac-like frequency, in Figure 3.9g. Here, the plane wave does not break after leaving from the PnCs in channels C1 and C2. After crossing the Dirac-like frequency, the wave gets segmented into 3 horn shaped patterns, keeping 2 linear portions of PnCs undisturbed on each side (Figure 3.9h). Hence, the wave transportation through PnC along MΓ direction shows verities of intriguing wave transportation and deviation phenomena.

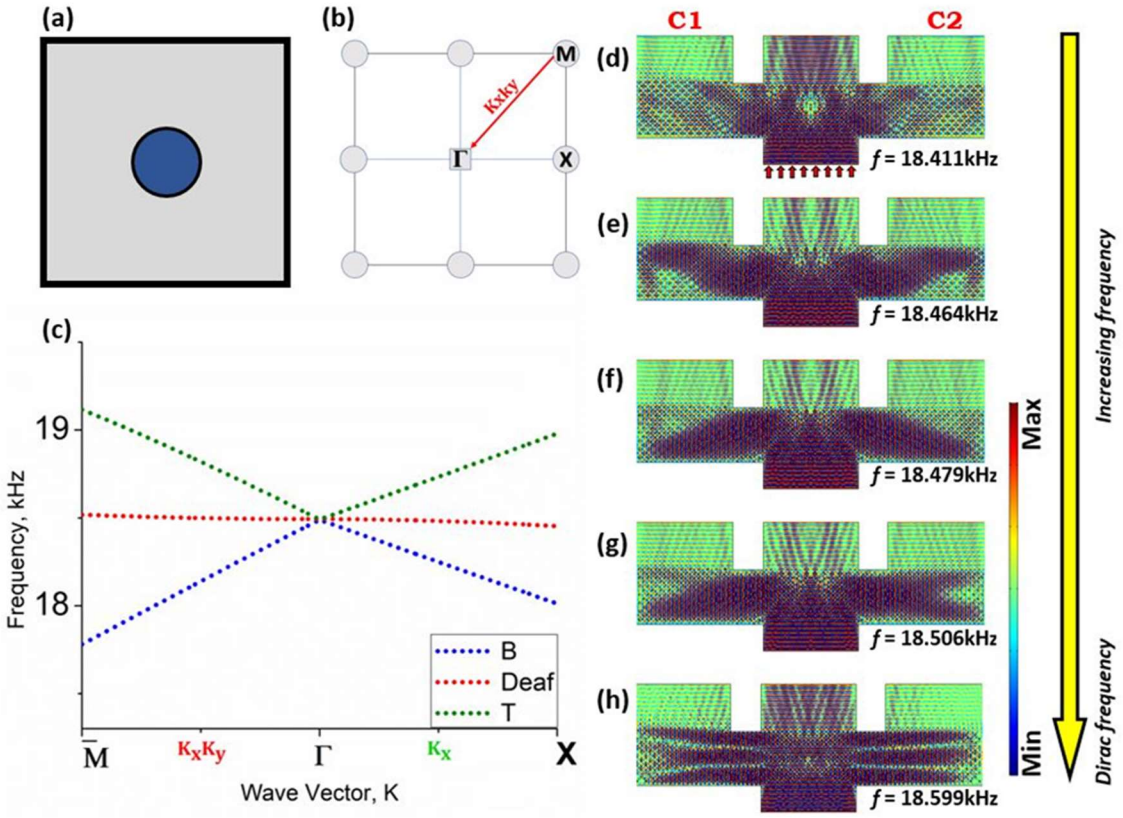

Figure 3.10: The unit cell of PnCs, (b) The first Brillouin zone structure, showing MΓ direction of wave vectors (c) The band structure showing Dirac-like point degenerated at f =~18.512 kHz at 'Region B', (d) to (h) the absolute acoustic pressure field for plane wave generated in ΓX direction for frequencies of f = ~18.196 kHz,18.336 kHz, 18.371 kHz, 18.468 kHz and 18.5 kHz respectively. Here we can see that, the wave has been transported orthogonally in a converging – diverging pattern when propagated at the Dirac like frequency of f = ~18.512 kHz

3.3.2.3 Formation of ‘No Zone’ - Propagation along MΓ

Figure 3.11a-b shows the close view of the acoustical wave field pattern, when the incident plane waves transported orthogonally inside the PnCs leaving two 45° bent lines. To form these bent lines, the incoming plane waves take a conical shape, and at the outer edges of the 2D conic make 45° angle to each other allowing the diversion of acoustic energy. As the acoustic energy diverts along these 45° bent lines, no or little amount of energy is left to divert at the intersection of these bent lines leaving some of the unit cells unaffected by the incoming or diverting plane waves. The region of PnCs where no acoustic energy is available at or near Dirac frequency is referred to as ‘No Zone’ in this article. The formation of ‘No Zone’ is at ~18.411 kHz in Figure 3.11b, which is close to the Dirac frequency, where a number of unit cells were unaffected and hence this area of the ‘No Zone’ becomes prominent. In Figure 3.11b, we can see that the ‘No Zone’ takes a square shape rotated in a 45^{O} rotation, where we have marked the ‘No Zone’ consisting of 9 PVC

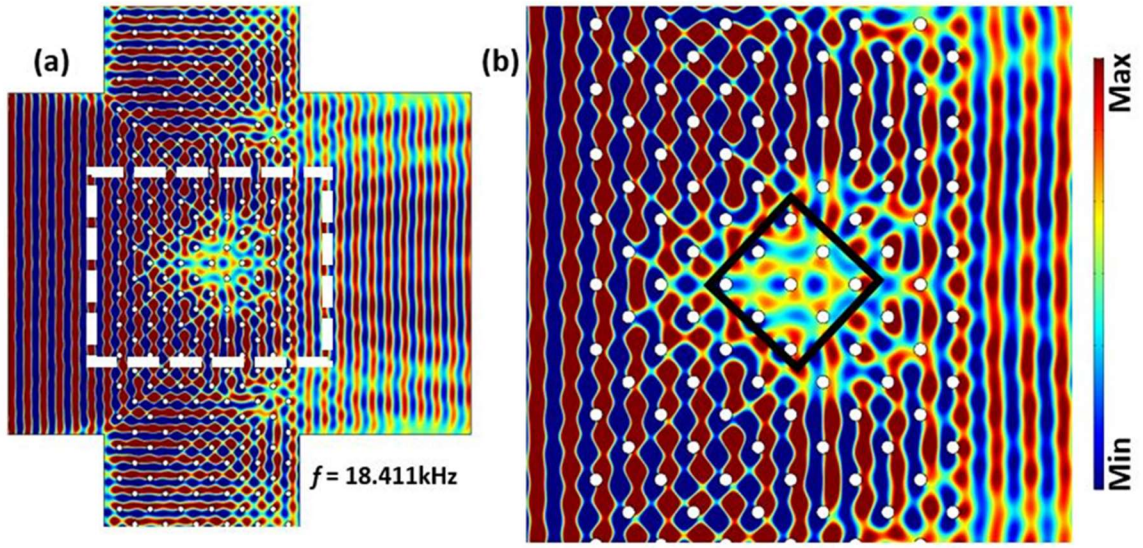

Figure 3.11: (a) The ‘No Zone’ that has been formed, at the center of the PnCs at f = ~18.411 kHz, (b) The zoomed-in region, showing a 'No Zone' at the verge of 4 bent lines, making a small region untouched by the plane waves

crystals. As actuation frequency increases and goes towards the Dirac frequency, the ‘No Zone’ area becomes smaller and disappear eventually.

CHAPTER 4

EXPERIMENTAL SETUP AND VALIDATION

An experimental design had been constructed to illustrate the Dirac-like features by modulating the radii of the PVC resonators. To validate the numerical results, it is sufficient to demonstrate orthogonal wave transportation and identify transmission coefficients at particular frequency points. Therefore, an experimental setup was constructed by commercially available extruded PVC rods as shown in Figure xx. A speaker capable of generating 12.551 kHz was excited using Tektronix function generator. To receive the transmitted wave out of the PnCs, dynamic pressure microphones were positioned at the designed output locations around the PnCs.

First, 140 commercially available extruded PVC cylinders, of r = 0.212a = 5.4 mm (The lattice constant a = 25.4 mm) were arranged in 10 x 14 matrix as shown in Figure 4.2. The PVC cylinders were cut in to 4" length elements and machined to have smooth surface to minimize the experimental errors. Before mounting all the PVC cylinders, we have bored 140 bores in one side of the acrylic sheet of depth of 5 mm each approximately. Then, PnCs have been arranged the PnCs in 10 x 14 matrix and generated the acoustic pressure excitation from one side, like given in Figure 4.1. Acoustic pressure was created from one side (Figure 4.2a & b) using a speaker (Pyle Gear (PLG 3.2) 3.5" 2-way coaxial, 120-watt, 4-ohm impedance) capable of generating frequencies up to 18 kHz was used. To absorb the acoustic energy at the boundaries to avoid reflection, acoustic dampers (foam sheets of

0.5-inch thick) were used along the boundary of the experimental setup (Figure 4.1d & e**).** Similar to the numerical study setup with absorbing boundary conditions, a channel made of foam was designed to guide the incident acoustic wave. The desired frequency ranges for validating orthogonal wave transportation at Dirac-like frequency is 12.5 – 12.7 kHz. A condenser pressure microphone (Sterling S30 Class-A FET 30 Hz-18 kHz) was used to detect the acoustic transmission (Figure 4.1 d & e), placed at an orthogonal (for OT) and

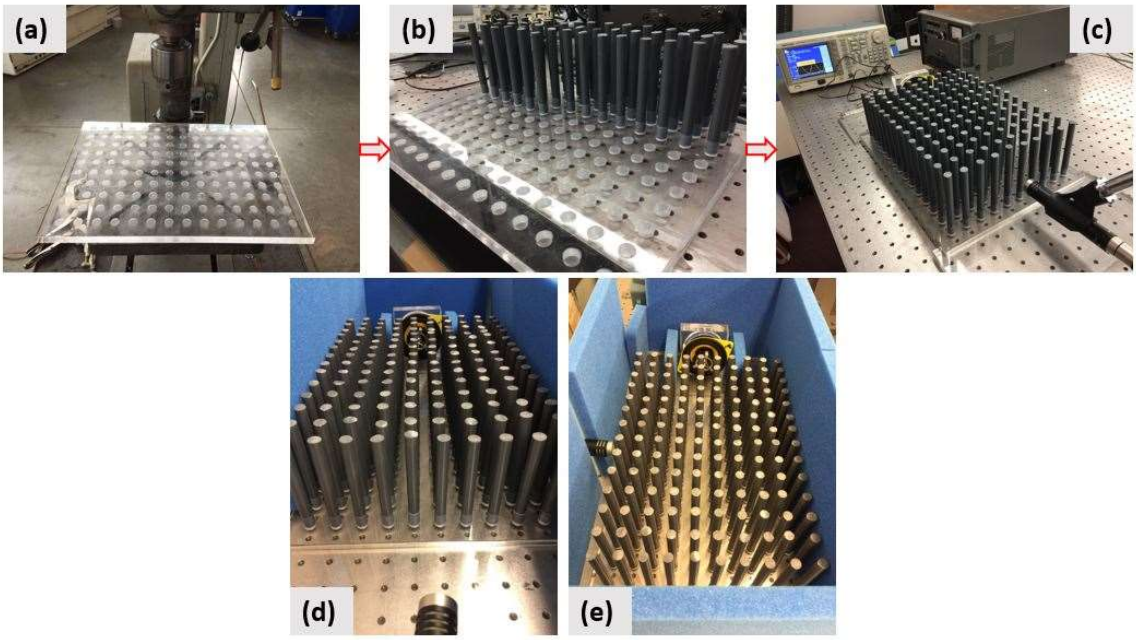

Figure 4.1: The experimental setup making process, (a) Acrylic sheet bored into 140 bores of 5mm depth each (approximately), (b) Placing PVC rods in the bores, (c) Establishing all the connections for the experimental setup, (d) and (e) Final setup with acoustic damper while the microphone is placed at 2 different directions.

incident (for IT) direction. The signal was collected, conditioned and processed using an acoustic signal conditioner.

Finally, the spectral analyses were performed to obtain the transmissibility at the IT and the OT locations. We have taken data from 2 different directions.

1. Transmission in Incident direction (IT)
2. Transmission in orthogonal direction (OT).

We have placed pressure microphones in both direction while allowing transmission through PnCs at 12.551 kHz. To help the acoustic energy gets absorbed and avoid reflected energy interference, acoustic damper has been used at the boundary of the PVC crystal setup. Foam sheet of 0.5-inch thickness has been used to serve this purpose. Like the numerical study setup, we have designed a guided channel for incident pressure wave to ensure the plane wave propagation phenomena. The angle of incidence of the plane wave needs to be along ΓX direction. If no channel is used, then the actuated wave become spherical wave which does not meet this requirement. Hence, we have used a channel made of foam for the actuating transducer.

Figure 4.2c shows the normalized transmissibility along IT and OT from the numerical and experimental study. It is clearly evident that the wave transmission along OT is significantly high compared to IT at or around the Dirac cone frequency. The complete experiment was repeated more than 10 times and the normalized spectral data presented are with the 98% confidence interval (shaded red and blue band) observed during the

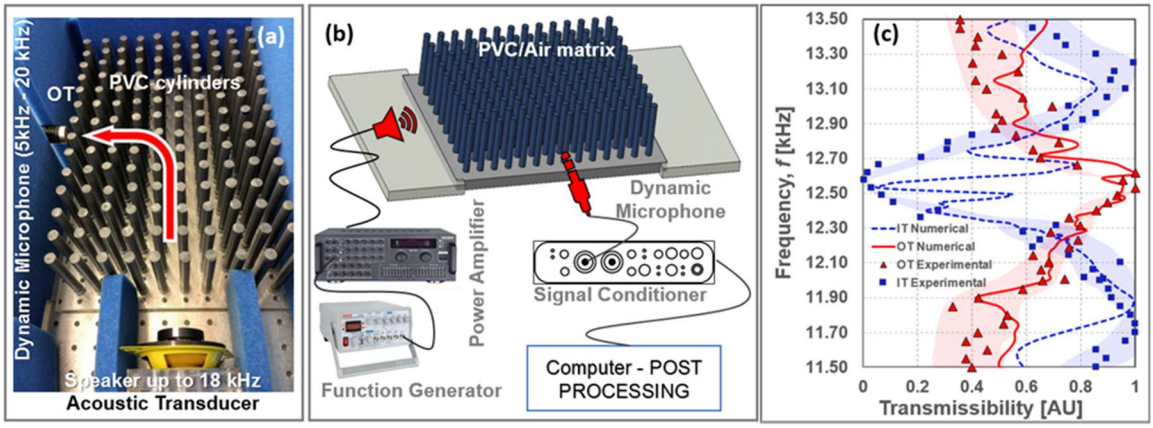

Figure 4.2: (a) Schematic flowchart of the experimental setup, (b) Experimental setup, (c) The comparison of numerical and experimental results of acoustic transmission (normalized) excited along ΓX direction for region A. The peak transmission is seen at Dirac like frequency for both numerical and experimental analysis.

experiment. Hence, this is conclusive that ‘deaf’ band based engineered Dirac cone was achieved and the orthogonal transport at Dirac frequency is eminent.

A maximum amount of transmission is observed along OT direction at Dirac-like frequency, along with the IT transmission being lowest. From Figure 4.2c, the comparison of transmission coefficient of numerical and experimental study has been given, where 90% of the data matches. Spectrum analysis was done to see the desired transmission coefficient for the range of frequencies actuated. We have run the experiment for frequency 10 – 14.5 kHz. For the convenience of the reader and better result showcasing, a normalized transmission has been shown in Figure ___ for the range of 12 – 13 kHz of transmission.

CHAPTER 5

DUAL DIRAC CONE GENERATION BY ANGLE BASED TUNING

5.1 Background

Dirac cone and double-Dirac cone, which have tremendous prospect in wave guiding and manipulating phenomena, has been studied and discussed till date. However, formation of dual Dirac cones at the center of the Brillouin zone, at different frequencies has never been reported in literature. Generation of multiple Dirac like cones at the center and the edge of a Brillouin zone, which is rare and, usually, non-manipulative is demonstrated in this article. By deploying variable angular position of the square PVC resonator as a unit cell in a phononic crystals (PC) system, the locations of the degenerated double Dirac cones have been manipulated at various frequency points. Gradual change in dispersion behavior as well as striking acoustic phenomena such as variable band gap, orthogonal wave transportation and wave trapping have been numerically demonstrated.

5.2 Angle based Tunable engineered PnCs

An angle based tunable engineered PnCs system has designed and reported here also. Generation of triply degenerated point at the center of Brillouin Zone (BZ) or Γ point is the result of accidental degeneracy. Though we have reported a way of making this accidental degeneracy a predictive or deterministic degeneracy in Chapter 3, but the actual

reason of this accidental degeneracy remains unknown. That is why, converting this 'accidental' phenomenon into a deterministic manner is the real challenge now. We have proposed a tunable engineered PnC system, where multiple Dirac-like points can be degenerated at Γ point. By tuning the solid resonator orientation with respect to the BZ. Similar to Chapter 3 study, keeping the mass constant, a simple square resonator has been designed, made of PVC, having a side of s = 0.342a. Here also the lattice constant has been considered as 1 inch (a = 1 inch). Square PVC inclusions were immersed in air media. A dispersion band structure was calculated numerically in a 2D study and multiple regions have been observed where a doubly-degenerated mode and a single mode is prevailing. After careful tuning of the structure by rotating clockwise changes the dispersion behavior of the crystals and helps to get degenerated into triply-degenerated points at multiple frequency locations for Γ.

Initially, the square PVC resonator, has been at an angle of 0 degree with respect to the lattice structure. Tuning the resonator by rotating it at an interval of 10 degrees, we

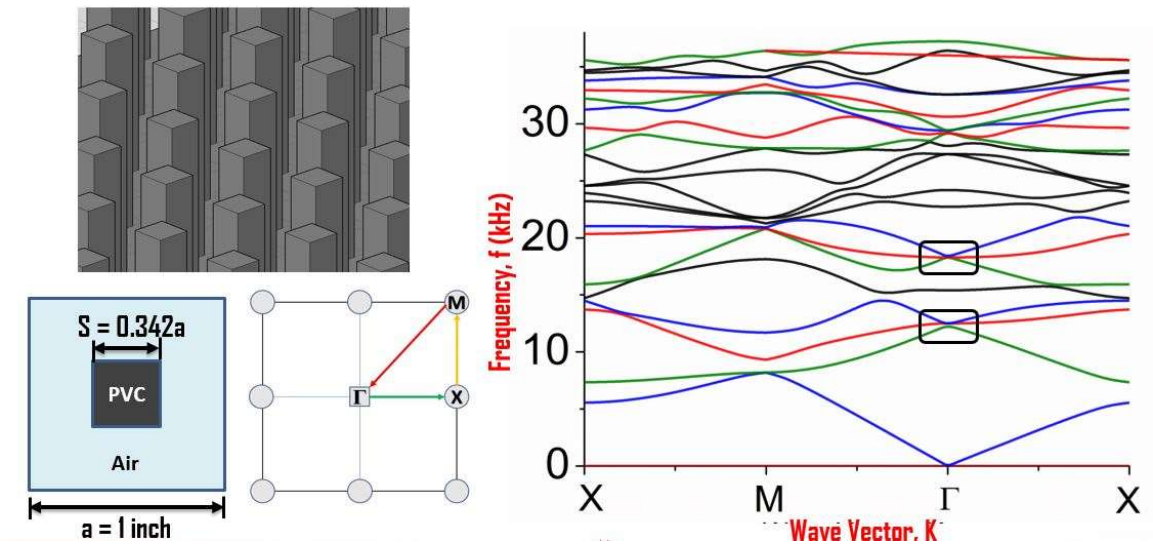

Figure 5.1: Sample band structure for square resonator of PVC inside air media, having a dimension of r = 0.342a where a = 1 inch.

found the band structure changing and the double degenerate modes generating with the single mode for some frequencies. The desired modes of getting triple degeneracy is shown in Figure 5.1. Carefully tuning the resonator, we obtain both the regions gets degenerated

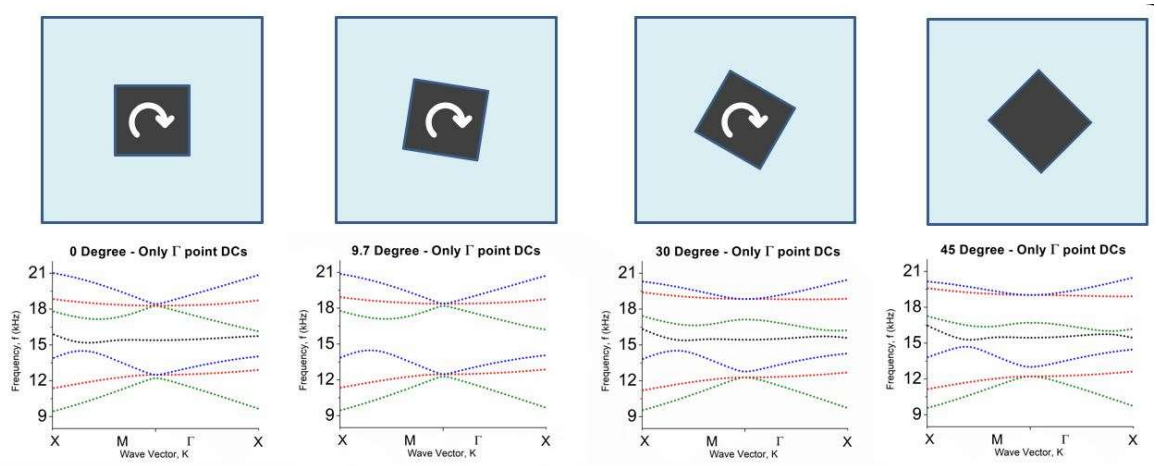

Figure 5.2: Gradual clockwise angular tuning is changing the wave dispersion, creating a dual Dirac cone formation at Γ point.

for the angle of 9.75 Degree of the resonator.

From Figure 5.2, the proper generation of Dirac-like cone can be observed for $\theta = 9.7\ Deg$. Generation of two Dirac-like cones at 2 close frequencies has never been reported before. Quadro-degenerated points have been reported where 4 bands intersect at a Dirac point, claiming that as a double Dirac-like cone. Here we have demonstrated the formation of dual Dirac cones at 2 different frequencies. The validation of the existence of Dirac-like point has also been confirmed by numerical frequency domain study for the structure. The frequency domain study has been done where the structure has been designed where orthogonal transportation can be realized. Cloaking effect can be easily observed by channeling PnCs orthogonally. Additionally, multiple Dirac cones can also be observed the corner of the BZ (M point) for this exact orientation. So, a single orientation of PVC

resonator can exhibit multiple Dirac cones and Dirac-like cones simultaneously, which can be used for wide verities of applications in air media.

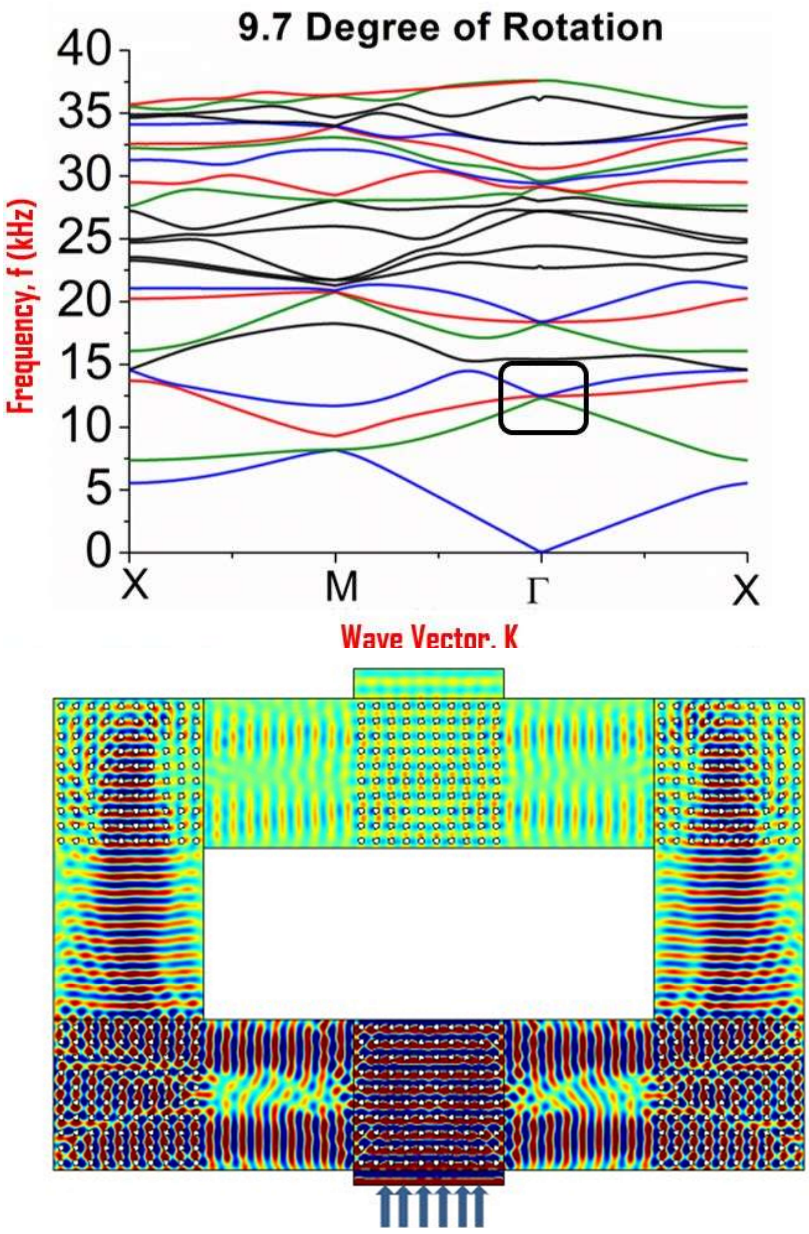

Figure 5.3: The triply degenerated point at Γ after tuning the resonator for $\theta = 9.7\ Deg$. Perfect orthogonal transportation can be observed at the acoustic pressure filed distribution when excited at the Dirac-like frequency.

Figure 5.3 shows the acoustic pressure field distribution of plane wave, excited at a frequency f = 12.505 kHz. This frequency is the Dirac frequency for the first Dirac-like point of the dual Dirac cone. Proper transmission along multiple orthogonal bends can be observed from Figure 5.3 which validates the existence of real Dirac-like point. An acoustic pressure excitation at a magnitude in terms of normal displacement of 0.1 m, has been given at the left boundary shown, and the wave manages to transmit along the orthogonal directions for 4 consecutive bends without getting decayed.

CHAPTER 6

ACOUSTIC TOPOLOGICAL CONDUCTION

6.1 Background

Topological insulator has been one of the intriguing topic of research for the past decade. The ability of transporting electrons only along the edge of a surface, prohibiting the transportation at the middle, is the prime phenomenon of topological insulators. Regardless of any deformation of the boundary, the edge transportation remains uninterrupted. That is why, they are called topologically protected. Recently, materials possessing topological properties have been found in nature. This has been one of the breakthrough discovery in the history of condensed matter physics. Till date, topological insulator has been researched in the area of photonics and condensed matter physics. In case of phononics and acoustics, this area is still to be covered and very less work have been done in this aspect. Like the way topological insulator is crucial in directional energy transportation, counter phenomena of topological insulator can also be considered as important.\

6.2 Methodology

Topological insulator helps to conduct electrons along the boundary of the material, where the rest of the material acts as an insulator, prohibiting conduction. Similarly, there

might be a phenomenon where the material acts like a conductor, keeping the boundary protected from the conduction. Here, the boundary exhibits insulating phenomena, keeping all the conduction away from the edge. We have developed a basic acoustic model where this phenomenon has been observed and that is why, we have proposed this phenomenon as "topological conduction". The counter phenomenon of topological insulator made us name it a topological conductor. If a PnC matrix is excited from one end at a certain frequency, the matrix acts like a topological conductor, keeping the edge safe from the acoustic energy propagation.

Acoustic energy excited at a frequency of 18.947 kHz creates topological conduction. We have generated the plane wave from the left boundary, shown in Figure 6.1. Here, the wave keeps travelling inside the PnCs, keeping the edge protected. A negligible amount of energy is leaking outside the PnCs which can be treated as a computational error. Now the material can be topologically protected when the edge

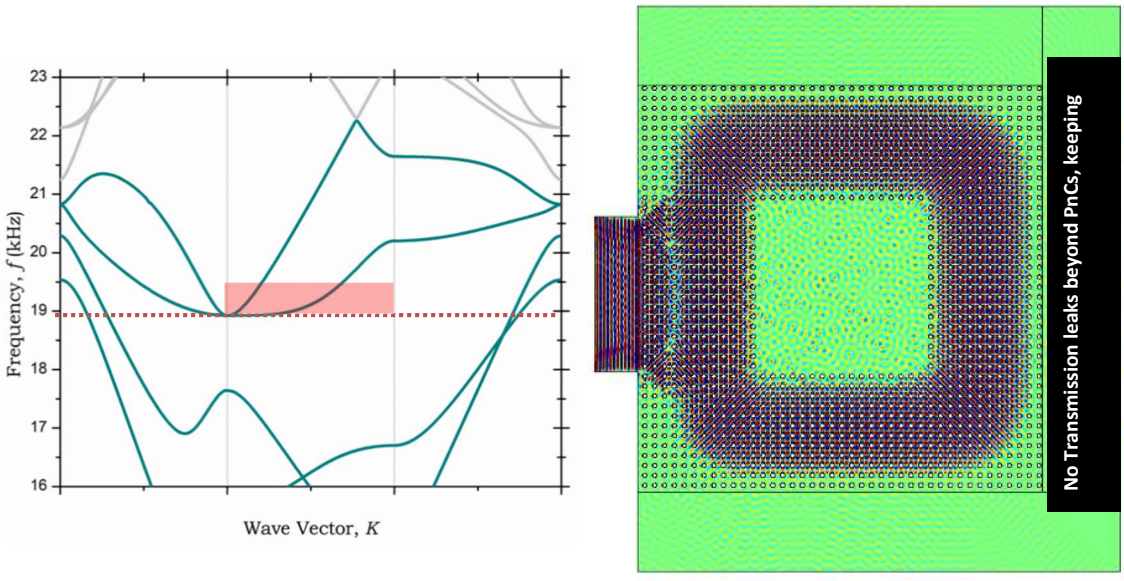

Figure 6.1: The band structure for the model of topological conduction phenomenon. A perfect topological conductor developed has been showed here where the acoustic energy is trapped and conducting inside the PnCs, keeping the boundaries unharmed and protected.

deformation does not vary the topological property of the material. We have changed the PnC matrix size and shape to observe the topological property of this topological conductor. We have found that, regardless of any shape and size, the topological properties remain unharmed and the PnCs remain topologically protected. Due to further study and finding for my PhD dissertation, I will keep this study up-to here.

CHAPTER 7

CONCLUSION AND FUTURE WORKS

In this study, we have analytically solved the dispersion behavior of PVC PnCs in air media, having multiple probable triple degeneracy at the Dirac-like point at $\vec{k} = 0$. We pivoted our study on two 'deaf bands' that are identified as probable governor of the Dirac–like cones. There we selected two frequency regions, to study further if the accidental degeneracies occur by modulating the physical parameter of the resonators. A predictive optimization process discussed in this article leads us to find the region of the Dirac-like cone based on the zero-group velocity flat bands, or the 'Deaf bands'. With this unique phenomenon depending on the deaf band, we fabricated two numerical experiments to determine the behaviors of the Dirac-like points, to test if the regions identified are actually the Dirac-like points. After test, we demonstrated that the orthogonal wave guidance at the Dirac points are evident in Region A and Region B. In this article, however, only the Region A Dirac point behaviors are discussed with several other phenomena like, orthogonal wave transport, channeling plane waves along the offset axes, acoustic No Zone, acoustic clocking, acoustic vortex or self-looping leaving imaginary acoustic sources at offset locations. Mode identification, relation between the mode shapes and their role in the above mentioned unique wave propagation behavior are logically analyzed and

discussed in this article. This this study, it will help us in the future to further find the intriguing wave guiding properties of Dirac cone in acoustic metamaterials.

REFERENCES

1. Zhang, X. and Z. Liu, *Extremal Transmission and Beating Effect of Acoustic Waves in Two-Dimensional Sonic Crystals.* Physical Review Letters, 2008. **101**(26): p. 264303.
2. Liu, F., et al., *Dirac cones at $\stackrel{P\vec}{k}=0$ in phononic crystals.* Physical Review B, 2011. **84**(22): p. 224113.
3. Liu, F., X. Huang, and C.T. Chan, *Dirac cones at k→=0 in acoustic crystals and zero refractive index acoustic materials.* Applied Physics Letters, 2012. **100**(7): p. 071911.
4. Mei, J., et al., *First-principles study of Dirac and Dirac-like cones in phononic and photonic crystals.* Physical Review B, 2012. **86**(3).
5. Lu, J., et al., *Dirac cones in two-dimensional artificial crystals for classical waves.* Physical Review B, 2014. **89**(13): p. 134302.
6. Huang, X., et al., *Dirac cones induced by accidental degeneracy in photonic crystals and zero-refractive-index materials.* Nat Mater, 2011. **10**(8): p. 582-6.
7. *The quantum theory of the electron.* Proceedings of the Royal Society of London. Series A, 1928. **117**(778): p. 610-624.
8. Zhang, X., *Observing Zitterbewegung for Photons near the Dirac Point of a Two-Dimensional Photonic Crystal.* Physical Review Letters, 2008. **100**(11): p. 113903.
9. Gusynin, V.P. and S.G. Sharapov, *Unconventional Integer Quantum Hall Effect in Graphene.* Physical Review Letters, 2005. **95**(14): p. 146801.
10. Torrent, D. and J. Sanchez-Dehesa, *Acoustic analogue of graphene: observation of Dirac cones in acoustic surface waves.* Phys Rev Lett, 2012. **108**(17): p. 174301.
11. Ochiai, T. and M. Onoda, *Photonic analog of graphene model and its extension: Dirac cone, symmetry, and edge states.* Physical Review B, 2009. **80**(15): p. 155103.
12. Malko, D., et al., *Competition for Graphene: Graphynes with Direction-Dependent Dirac Cones.* Physical Review Letters, 2012. **108**(8): p. 086804.
13. Zhang, Y., et al., *Experimental observation of the quantum Hall effect and Berry's phase in graphene.* Nature, 2005. **438**: p. 201.
14. Ziolkowski, R.W., *Propagation in and scattering from a matched metamaterial having a zero index of refraction.* Physical Review E, 2004. **70**(4): p. 046608.
15. Huang, X., et al., *Dirac cones induced by accidental degeneracy in photonic crystals and zero-refractive-index materials.* Nature materials, 2011. **10**(8): p. 582.
16. Hossain, A., et al., *Multifunction acoustic modulation by a multi-mode acoustic metamaterial architecture.* Journal of Physics Communications, 2018. **2**(11): p. 115001.
17. Li, Y., et al., *Selection rule for Dirac-like points in two-dimensional dielectric photonic crystals.* Optics Express, 2013. **21**(6): p. 7699-7711.

18. Chen, Z.-G. and Y. Wu, *Tunable Topological Phononic Crystals.* Physical Review Applied, 2016. **5**(5).
19. Islam, A.B.M.I. and A.D. Kelkar, *Fabrication and Characterization of Nanofiber Enhanced Prepregs.* MRS Advances, 2017. **2**(17): p. 951-956.
20. Shelke, A., et al., *Wave guiding and wave modulation using phononic crystal defects.* Journal of Intelligent Material Systems and Structures, 2014. **25**(13): p. 1541-1552.
21. Fatima, M. Zepeda, and N. Oncel, *Scanning tunneling microscopy/spectroscopy measurements and density functional theory calculations on self-assembled monolayer of octanoic acid on graphite.* Thin Solid Films, 2017. **623**: p. 135-137.
22. Fatima, u., et al., *First-Principles Study of Charge Carrier Dynamics with Explicit Treatment of Momentum Dispersion on Si Nanowires along <211> crystallographic Directions.* MRS Advances, 2018. **3**(59): p. 3477-3482.
23. Psarobas, I., et al., *Acoustic properties of colloidal crystals.* Physical Review B, 2002. **65**(6): p. 064307.
24. Sánchez-Pérez, J.V., et al., *Sound Attenuation by a Two-Dimensional Array of Rigid Cylinders.* Physical Review Letters, 1998. **80**(24): p. 5325-5328.
25. Islam, A.I., *Monitoring Wear in Sliding Surfaces by Using Acoustic Emission Signals*. 2013, North Carolina Agricultural and Technical State University.
26. Indaleeb, M., H. Ahmed, and S. Banerjee. *Investigation on multi-occurrence of Dirac cone and exceptional ring (Conference Presentation)*. in *SPIE Smart Structures and Materials + Nondestructive Evaluation and Health Monitoring*. 2018. SPIE.
27. Ahmed, H., et al., *Investigation and development of friction stir welding process for unreinforced polyphenylene sulfide and reinforced polyetheretherketone.* Journal of Thermoplastic Composite Materials, 2018: p. 0892705718785676.
28. Patra, S., H. Ahmed, and S. Banerjee, *Peri-Elastodynamic Simulations of Guided Ultrasonic Waves in Plate-Like Structure with Surface Mounted PZT.* Sensors, 2018. **18**(1): p. 274.
29. Kafesaki, M., R. Penciu, and E. Economou, *Air bubbles in water: a strongly multiple scattering medium for acoustic waves.* Physical review letters, 2000. **84**(26): p. 6050.
30. Liu, Z., et al., *Elastic wave scattering by periodic structures of spherical objects: Theory and experiment.* Physical Review B, 2000. **62**(4): p. 2446.
31. Psarobas, I., N. Stefanou, and A. Modinos, *Scattering of elastic waves by periodic arrays of spherical bodies.* Physical Review B, 2000. **62**(1): p. 278.
32. Psarobas, I., N. Stefanou, and A. Modinos, *Phononic crystals with planar defects.* Physical Review B, 2000. **62**(9): p. 5536.
33. Deymier, P., *Acoustic Metamaterial and Phononic Crystals.* Springer series in solid state sciences, 2013. **173**.
34. Tanaka, Y., Tomoyasu, Y., Tamura, S., , *Band structure of acoustic waves in phononic lattices: Two-dimensional composites with large acoustic mismatch* Physical Review B, 2000. **62**(11): p. 7387-7392.
35. Bucay, J., et al., , *Positive, negative, zero refraction, and beam splitting in a solid/air phononic crystal: Theoretical and experimental study.* Physical Review B, 2009. **79**: p. 214305-1-7.

36. Pennec, Y., et al., *Two-dimensional phononic crystals: Examples and applications.* Surface Science Reports, 2010. **65**: p. 229-291.
37. Hussein, M.I., *Reduced Bloch mode expansion for periodic media band structure calculations.* Proceedings of the Royal Society A: Mathematical, Physical and Engineering Science, 2009. **465**(2109): p. 2825-2848.
38. Rubio, J.E., P. Sarker, and U.K. Chakravarty, *Characterization of the Electromechanical Response of a Dielectric Elastomer Membrane.* 2014(46590): p. V010T13A016.
39. Li, J. and C.T. Chan, *Double-negative acoustic metamaterial.* Physical Review E, 2004. **70**(5): p. 055602.
40. Robertson, W., et al., *Measurement of photonic band structure in a two-dimensional periodic dielectric array.* Physical review letters, 1992. **68**(13): p. 2023.
41. Chen, Z.-G., et al., *Accidental degeneracy of double Dirac cones in a phononic crystal.* Scientific Reports, 2014. **4**: p. 4613.
42. Sánchez-Pérez, J.V., et al., *Sound attenuation by a two-dimensional array of rigid cylinders.* Physical Review Letters, 1998. **80**(24): p. 5325.
43. Hsiao, F.-L., et al., *Complete band gaps and deaf bands of triangular and honeycomb water-steel phononic crystals.* Journal of applied physics, 2007. **101**(4): p. 044903.